Appendix A

General formulation of conventional numerical methods

A.1 Introduction

The general formulation of *continuum* and *discontinuum* methods, as well as the simulation of fracture process using different numerical tecniques, described in this appendix, is based on the previous work made by Jing (2003).

A.2 Numerical methods in rock engineering

In rock engineering several modelling methods have been developed for the study and design of rock engineering structures. In the literature these approaches are divided into two main groups which differ for the type of representation of the problem used.

In the *discrete representation*, engineering problems are represented by an adequate model using a finite number of well-defined components. The behaviour of such components is either well known, or can be independently treated mathematically. The global behaviour of the system can be determined through well-defined inter-relations between the individual components (elements). In such problems, termed *discrete,* the discrete representation and solution of such systems by numerical methods are usually straightforward.

In other problems, the definition of such independent components may require an infinite sub-division of the problem domain, and the problem can only be treated using the

mathematical assumption of an *infinitesimal element*, implying in theory an infinite number of components. This usually leads to differential equations to describe the system behaviour at the field points. Such systems are termed *continuous representation* and have infinite degrees of freedom. To solve such a continuous problem by numerical methods, the problem domain is usually subdivided into a finite number of sub-domains (elements) whose behaviour is approximated by simpler mathematical descriptions with finite degrees of freedom. These sub-domains must satisfy both the governing differential equations of the problem and the continuity condition at their interfaces with adjacent elements. This is the so-called discretization of a continuum. It is an approximation of a continuous system with infinite degrees of freedom by a discrete system with finite degrees of freedom. The continuum assumption implies that at all points in a problem domain, the materials cannot be torn open or broken into pieces. Of course, at the microscopic scale, all materials are discrete systems. However, representing the microscopic components individually is intractable mathematically and unnecessary in practice.

The concepts of *continuum* and *discontinuum* are therefore not absolute but relative, depending especially on the problem scales. Due to the differences in the underlying material assumptions, different numerical methods have been developed for *continuous* and *discrete* systems. The most commonly applied numerical methods for rock mechanics problems are:

continuum methods

- FINITE DIFFERENCE METHOD (FDM). The FDM method is the oldest numerical method, and it is the basis of the explicit approach of the DEMs. The FDM is a direct approximation of the governing Partial Differential Equations (PDEs) by replacing partial derivatives with differences at regular or irregular grids imposed over problem domains. The solution of the system equation is obtained after imposing the initial and boundary conditions;

- FINITE ELEMENT METHOD (FEM). The FEM is perhaps the most widely applied numerical method in engineering because its flexibility in handling material heterogeneity, non-linearity and boundary conditions. It is also the basis of the implicit approach of the DEM. The FEM requires the division of the problem domain into sub-domains (elements) of standard shapes (triangle, quadrilateral, tetrahedral, etc.) with fixed number of nodes at the vertices and/or on the sides. Polynomial functions are used to approximate the behaviour of PDEs at the element level and generate the local algebraic equations representing the behaviour of the elements. The local elemental equations are then assembled, according to the topologic relations between the nodes and elements, into a global system of algebraic

equations whose solution then produces the required information in the solution domain, after imposing the properly defined initial and boundary conditions;

- BOUNDARY ELEMENT METHOD (BEM). The BEM requires discretization at the boundary of the solution domains only. The information required in the solution domain is separately calculated from the information on the boundary, which is obtained by solution of a boundary integral equation, instead of direct solution of the PDEs, as in the FDM and FEM. It has greater accuracy over the FDM and FEM at the same level of discretization and is also the most efficient technique for fracture propagation analysis.

discontinuum methods

- DISCRETE ELEMENT METHOD (DEM). The DEM for modelling a discontinuum focuses mostly on applications in the fields of fractured geological media. The DEM represents the fractured medium as assemblages of blocks connected by fractures. The equations of motion of these blocks are solved through continuous detection and treatment of contacts between the blocks. The blocks can be rigid or be deformable with FDM or FEM discretizations. Large displacements caused by rigid body motion of individual blocks, including block rotation, fracture opening and complete detachments is straightforward in the DEM, but impossible in the FDM, FEM or BEM;

- DISCRETE FRACTURE NETWORK (DFN) method. The DFN method is an alternative DEM for fluid flow in fractured rock masses. It simulates fluid flow through connected fracture networks, with the matrix permeability either ignored or approximated by simple means. The stress and deformation of the fractures are generally ignored as well. This method is conceptually attractive for simulating fluid flow in fractured rocks when the permeability of the rock matrix is low compared to that of the fractures.

hybrid continuum/discontinuum models

- Hybrid FEM/BEM;

- Hybrid DEM/DEM;

- Hybrid FEM/DEM, and

- Other hybrid models.

A.3   Continuum methods

A.3.1   FINITE DIFFERENCE METHOD (FDM)

The FDM is the oldest numerical method to obtain approximate solutions to PDEs in engineering. The basic concept of FDM is to replace the partial derivatives of the object-ive function (e.g. displacement) by differences defined over certain spatial intervals in the coordinate directions Δx, Δy, $\triangle z$, which yields a system of algebraic simultaneous equations of the objective functions at a grid (mesh) of nodes over the domain of interest (Figure A.1) (Wheel, 1996). Solution of the simultaneous algebraic system equations, incorporating boundary conditions defined at boundary nodes, will then produce the required values of the objective function at all nodes, which satisfy both the governing PDFs and specified boundary conditions. The conventional FDM utilizes a regular grid of nodes, such as a rectangular grid as shown in Figure A.1a.

Using a standard FDM scheme, the so-called 5-point difference scheme (Figure A.1b), the resultant FDM equation at grid node (i, j) will be expressed as combinations of func-tion values at its four surrounding nodes. For a Navier equation of equilibrium for elastic solids in 2D, the FDM equation of equilibrium at point (i, j) is given as

$$u_x^{i,j} = a_1 u_x^{i-1,j} + a_2 u_x^{i,j-1} + a_3 u_x^{i,j+1} + a_4 u_x^{i+1,j} + a_5 u_x^{i+1,j+1} + a_6 F_x^{i,j}$$
$$u_y^{i,j} = b_1 u_y^{i-1,j} + b_2 u_y^{i,j-1} + b_3 u_y^{i,j+1} + b_4 u_y^{i+1,j} + b_5 u_y^{i+1,j+1} + b_6 F_y^{i,j} \tag{A.1}$$

where coefficients a_k and b_k $(k = 1, 2, ..., 6)$ are functions of the grid intervals Δx and Δy and the elastic properties of the solids, and $F_x^{i,j}$ and $F_y^{i,j}$ are the body forces lumped at point (i, j), respectively. Assembly of similar equations at all grid points will yield a global system of algebraic equations whose solution can be obtained by direct or iterative methods. FDM schemes can also be applied in the time domain with properly chosen time steps, Δt, so that function values at time t can be inferred from values at $t - \Delta t$.

The fundamental nature of FDM is the direct discretization of the governing PDEs by replacing the partial derivatives with differences defined at neighboring grid points. The grid system is only a convenient way of generating objective function values at sampling points with small enough intervals between them, so that errors thus introduced are small enough to be acceptable. No local trial (or interpolation) functions are employed to approximate the PDE in the neighborhoods of the sampling points, as is done in FEM and BEM.

The conventional FDM with regular grid systems does suffer from shortcomings, most of all in its inflexibility in dealing with fractures, complex boundary conditions and material inhomogeneity. This makes the standard FDM generally unsuitable for
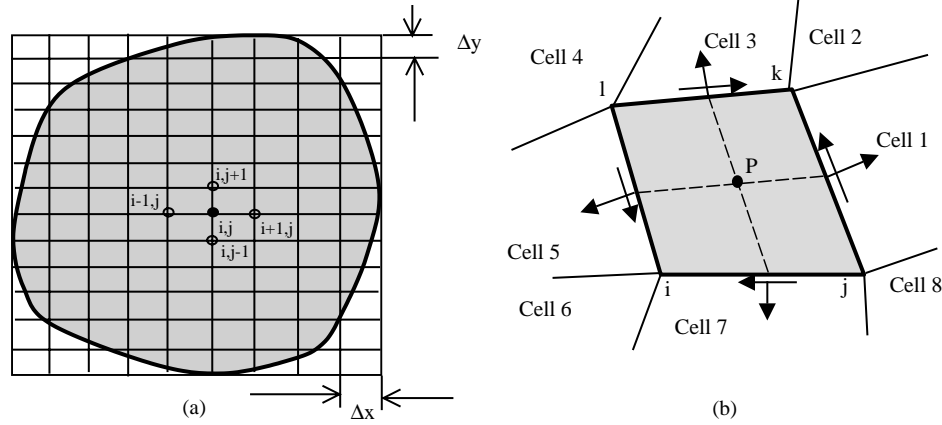
Figure A.1: (a) Regular quadrilateral grid for the FDM and (b) irregular quadrilateral grid for the FVM (Wheel, 1996).

modeling practical rock mechanics problems. However, significant progress has been made in the FDM so that irregular meshes, such as quadrilateral grids (Perrone and Kao, 1975) and the Voronoi grids (Brighi et al., 1998) can also be used. Although such irregular meshes can enhance the applicability of the FDM for rock mechanics problems, however, the most significant improvement comes from the so-called Control Volume or Finite Volume approaches.

A.3.1.1 Finite volume approach of FDM and its application to stress analysis

The Finite Volume Method (FVM) is also a direct approximation of the PDEs, but in an integral sense. An elastostatic problem with body Ω, is divided into a finite number, N, of internal contiguous cells of arbitrary polyhedral (or polygonal in 2D cases) shape, called Control Volumes (CV), Ω_k, with boundary Γ_k, of unit outward normal vector n_i^k, $k = 1, 2, ..., N$. The boundary Γ_k of Ω_k is comprised of a number, M^k, polygonal side (faces or line segments), Γ_k^p, $p = 1, 2, ..., M^k$. Assuming isotropic, linear elasticity and using Gauss' divergence theorem, the Navier–Cauchy equation of equilibrium in terms of stress can be rewritten in terms of displacement as

$$\sum_{k=1}^{N} \left[\sum_{p=1}^{M^k} \int_{\Gamma_k^p} t_i^k d\Gamma + \int_{\Omega_k} f_i d\Omega \right] = \sum_{k=1}^{N} \left[\sum_{p=1}^{M^k} \int_{\Gamma_k^p} \sigma_{ij}^k n_j^p d\Gamma + F_x^k \right] = 0 \qquad \text{(A.2)}$$

where $F_i^k = \rho g_i V^k$ is the body force vector of the CV of volume V^k lumped at its center, ρ is the material density and g_i is the body force intensity vector, such as gravity acceleration.

The task is to formulate the integrals into algebraic functions of the displacements at nodes defining the boundary sides Γ_k^p of Ω_k, which vary with different grid schemes. For an unstructured quadrilateral grid system (Figure A.1b), a typical cell P (CV), with its center at node P, has four sides (ij, jk, kl, li) and four nodes (i, j, k, l), surrounded by eight neighboring cells with center nodes $I, J, ..., O$. The integral terms in Equation A.2 for the cell P are written in terms of displacement variables at the centers of cells (Wheel, 1996), written as

$$A_p u_x^p + \sum_r A_r u_x^r + B_p u_y^p + \sum_r B_r u_y^r + F_x^K$$

$$C_p u_y^p + \sum_r C_r u_y^r + D_p u_x^p + \sum D_r u_x^r + F_y^K \qquad \text{(A.3)}$$

where coefficients $A_p, A_r, B_p, B_r, C_p, C_r, D_p, D_r$ are functions of the cell geometry and the elastic properties of the solids, with $r = 1, 2, ..., 8$ running through the eight surrounding cells.

The FDM/FVM approach is therefore as flexible as FEM in handling material inhomogeneity and mesh generation. As a branch of the FDM, the FVM can overcome the inflexibility of the grid generation and boundary conditions in the traditional FDM with unstructured grids of arbitrary shape.

The FDM/FVM approaches are therefore specially suited to simulate non-linear behavior of solid materials. The reason is its special advantage of no-matrix-equation-solving formulation and data structure, so that integration of non-linear constitutive equations is a straightforward computer implementation step, rather than iterative prediction-mapping integration loops required in FEM.

At present, the most well-known computer codes for stress analysis for non-linear rock engineering problems using the FVM/FDM approach is perhaps the FLAC code group (ITASCA Consulting Group, 1993b), with a vertex scheme of triangle or quadrilateral grids.

A.3.2 Finite Element Method (FEM)

The FEM requires the division of the problem domain into a collection of sub-domains (elements) of smaller sizes and standard shapes (triangle, quadrilateral, tetrahedral, etc.) with fixed number of nodes at the vertices and/or on the sides, the discretization. Trial functions, usually polynomial, are used to approximate the behavior of PDEs at the element level and generate the local algebraic equations representing the behavior of the elements. The local elemental equations are then assembled, according to the topologic relations between the nodes and elements, into a global system of algebraic equations whose solution then produces the required information in the solution domain, after imposing the properly defined initial and boundary conditions.

The FEM has been the most popular numerical method in engineering sciences, including rock mechanics and rock engineering. Its popularity is largely due to its flexibility in handling material inhomogeneity and anisotropy, complex boundary conditions and dynamic problems, together with moderate efficiency in dealing with complex constitutive models and fractures. All these merits were very appealing to researchers and practicing engineers alike during early development in the 1960s and 1970s when the main numerical method in engineering analysis was the FDM with regular grids. Since then, the FEM method has been extended in many directions.

Basically, three steps are required to complete an FEM analysis:

1. domain discretization;

2. local approximation;

3. assemblage and solution of the global matrix equation.

The domain discretization involves dividing the domain into a finite number of internal contiguous elements of regular shapes defined by a fixed number of nodes (e.g., triangle elements with three nodes in 2D and brick elements with eight nodes in 3D). A basic assumption in the FEM is that the unknown function, u_i^e over each element, can be approximated through a trial function of its nodal values of the system unknowns, u_i^j, in a polynomial form. The trial function must satisfy the governing PDF and is given by

$$u_i^e = \sum_{j=1}^{M} N_{ij} u_i^j \tag{A.4}$$

where the N_{ij} are often called the shape functions (or interpolation functions) defined in intrinsic coordinates in order to use Gaussian quadrature integration, and M is the order

of the elements. Using the shape functions, the original PDF of the problem is replaced by an algebraic system of equations written as

$$\sum_{i=1}^{N} \left[K_{ij}^{e} \right] \left\{ u_{j}^{e} \right\} = \sum_{i=1}^{N} \left(f_{i}^{e} \right) \quad or \quad \mathbf{Ku} = \mathbf{F} \tag{A.5}$$

where matrix $\left[K_{ij}^{e} \right]$ is the coefficient matrix, vector $\left\{ u_{j}^{e} \right\}$ is the nodal value vector of the unknown variables, and vector $\left\{ f_{i}^{e} \right\}$ is comprised of contributions from body force terms and initial/boundary conditions.

For elasticity problems, the matrix $\left[K_{ij}^{e} \right]$ is called the element stiffness matrix given by

$$\left[K_{ij}^{e} \right] = \int_{\Omega_{i}} \left([B_{i}] [N_{i}] \right)^{T} \left([D_{i}] [B_{j}] \right) d\Omega \tag{A.6}$$

where matrix $[D_i]$ is the elasticity matrix and matrix $[B_i]$ is the geometry matrix determined by the relation between the displacement and strain. The global stiffness matrix **K** is banded and symmetric because the matrices $[D_i]$ are symmetric. Material inhomogeneity in FEM is most straightforwardly incorporated by assigning different material properties to different elements (or regions). To enforce the displacement compatibility condition, the order of shape functions along a common edge shared by two elements must be the same, so that no displacement discontinuity occurs along and across the edge.

"Infinite elements" have also been developed in FEM to consider the effects of an infinite far-field domain on the near-field behavior, most notably the "infinite domain elements" of Beer and Meek (1981) and the "mapped infinite elements" of Zienkiewicz et al. (1983), with focus on geomechanical applications. The mapped infinite elements are simply implemented using special shape functions that project boundary nodes at infinite distances in one or two directions, where the displacements are either zero or have prescribed values. Additional nodes are needed at the imaginary infinite locations. The infinite domain element technique does not require additional infinite nodes, but requires a "decay function" to describe the manner in which the displacements vary from mesh boundary to infinity. The shape functions used in the infinite element formulations are singular at the "infinite" nodes.

A.3.3   BOUNDARY ELEMENT METHOD (BEM)

The BEM requires discretization at the boundary of the solution domains only, thus reducing the problem dimensions by one and greatly simplifying the input requirements. The

information required in the solution domain is separately calculated from the information on the boundary, which is obtained by solution of a boundary integral equation, instead of direct solution of the PDEs, as in the FDM and FEM.

Unlike the FEM and FDM methods, the BEM approach initially seeks a weak solution at the global level through an integral statement, based on Betti's reciprocal theorem and Somigliana's identity. For a linear elasticity problem with domain Ω boundary Γ of unit outward normal vector n_i and constant body force f_i for example, the integral statement is written as

$$c_{ij}u_j + \int_\Gamma t_{ij}^* u_j d\Gamma = \int_\Gamma u_{ij}^* t_j d\Gamma + \int_\Gamma \frac{\partial u_{ij}^*}{\partial n} f_j d\Gamma \tag{A.7}$$

where u_j and t_j are the displacement and traction vectors on the boundary Γ the terms u_{ij}^* and t_{ij}^* are called displacement and traction kernels. The term c_{ij} is called the free term determined by the local geometry of the boundary surfaces, $c_{ij} = 1$ when the field point is inside the domain Ω. The solution of the integral Equation A.7 requires the following steps:

1. *Discretization of the boundary Γ with a finite number of boundary elements.* For 2D problems, the elements are 1D line segments which may have one node at the center of the element (constant element), two nodes at the two ends of the line segment (linear elements) or three nodes with two end nodes and one central node (quadratic elements). Let N denote the total number of boundary elements. The boundary integral equation then is re-arranged into a sum of local integrals over all elements

$$c_{ij}u_j + \sum_{k=1}^N \int_{\Gamma_k} t_{ij}^* u_j d\Gamma = \sum_{k=1}^N \int_{\Gamma_k} u_{ij}^* t_j d\Gamma + \sum_{k=1}^N \int_{\Gamma_k} \frac{\partial u_{ij}^*}{\partial n} f_j d\Gamma \tag{A.8}$$

2. *Approximation of the solution of functions locally at boundary elements by (trial) shape functions*, in a similar way to that used for FEM. The difference is that only 1D shape functions with intrinsic coordinate $-1 \leqslant \xi \leqslant 1$ is needed for 2D BEM problems, and 2D shape functions with two intrinsic coordinates $-1 \leqslant \xi \leqslant 1$ and $-1 \leqslant \eta \leqslant 1$ are needed for 3D problems. The displacement and traction functions within each element are then expressed as the sum of their nodal values of the element nodes:

$$u_i = \sum_{k=1}^m N_k u_i^k, \quad u_i = \sum_{k=1}^m N_k t_i^k \tag{A.9}$$

where m is the element order ($m = 1, 2 \text{ or } 3$ for 2D problems, for example), and u_i^k and t_i^k are the nodal displacement and traction values at node k, respectively.

Substitution of Equations A.9 into Equation A.8 and for

$$T_{ij} = \int_{\Gamma_k} t_{ij}^* N_j d\Gamma, \quad U_{ij} = \int_{\Gamma_k} u_{ij}^* N_j d\Gamma,$$
$$B_{ij} = \int_{\Gamma_k} f_j \frac{\partial u_{ij}^*}{\partial n} d\Gamma \tag{A.10}$$

Equation A.7 can be written in matrix form as

$$\begin{bmatrix} T_{ij}(l,k) \end{bmatrix} \{u_j(k)\} = \begin{bmatrix} U_{ij}(l,k) \end{bmatrix} \{t_j(k)\} + \{B_i(k)\}$$
$$(2N \times 2N)\ (2N \times 1)\ (2N \times 2N)\ (2N \times 1)\ (2N \times 1) \tag{A.11}$$

where $i, j = 1, 2$ for 2D and $i, j = 1, 2, 3$ for 3D problems, respectively, $l, k = 1, 2, ..., N$ and

$$T_{ij}(l,k) = c_{ij}\delta_{lk} + \int_{\Gamma_k} t_{ij}^* N_j d\Gamma \tag{A.12}$$

3. *Evaluation of the integrals T_{ij}, U_{ij} and B_i with point collocation method by setting the source point P at all boundary nodes successively.*

4. *Incorporation of boundary conditions and solution.* Incorporation of the boundary conditions into the matrix (Equation A.11) will lead to final matrix equation

$$[A]\{x\} = \{b\} \tag{A.13}$$

where the global matrix $[A]$ is a mixture of T_{ij}, and U_{ij}, the unknown vector (x) is a composite of both unknown displacements and unknown boundary tractions, and the known vector $\{b\}$ is the sum of the body force vector $\{B_i\}$ and the products of T_{ij} with known displacements and U_{ij} with known tractions, respectively. The resultant Equation A.13 is usually fully populated and asymmetric, leading to fewer choices for efficient equation solvers, compared with the sparse and symmetric matrices encountered in the FEM. The solution of Equation A.13 will yield the values of unknown displacements and tractions at boundary nodes. Therefore all boundary values of displacements and tractions are obtained.

5. *Evaluation of displacements and stresses inside the domain.* For practical problems, it is often the stresses and displacements at some points inside the domain of interest that have special significance. Unlike the FEM in which the desired data are automatically produced at all interior and boundary nodes, whether some of them are needed or not, in BEM the displacement and stress values at any interior point, P must be evaluated separately by

$$u_i(P) = -\sum_{k=1}^{M} \hat{T}_{ij} \bar{u}_j^k + \sum_{k=1}^{M} \hat{U}_{ij} \bar{t}_j^k + \sum_{k=1}^{M} \hat{B}_k \tag{A.14}$$

$$\sigma_{ij}(P) = -\sum_{l=1}^{M} S_{kij}\bar{u}_k^l + \sum_{l=1}^{M} D_{kij}\bar{t}_k^l \qquad (A.15)$$

where kernels $\hat{T}_{ij}$, $\hat{U}_{ij}$, S_{kij}, D_{kij} and $\hat{B}_i$ must be reevaluated according to the new position of the source point inside the domain (closed-form formula for them are available in many text books on the BEM), usually without singularities unless the point is very close to boundary, and $\bar{u}_j^k$ and $\bar{t}_j^k$ are known or calculated displacement and traction vectors at all boundary nodes.

The main advantage of the BEM is the reduction of the computational model dimension by one, with much simpler mesh generation and therefore input data preparation, compared with full domain discretization methods such as the FEM and FDM. Using the same level of discretization, the BEM is often more accurate than the FEM and FDM, due to its direct integral formulation. In addition, solutions inside the domain are continuous, unlike the point wise discontinuous solutions obtained by the FEM and FDM groups. The solution domains of BEM can be divided into several sub-domains with different material properties, and this will often reduce the calculation time as well. The method is also suitable for considering infinite domains (full or half space/plane), due to its use of the fundamental solutions.

However, in general, the BEM is not as efficient as the FEM in dealing with material heterogeneity, because it cannot have as many sub-domains as elements in the FEM. The BEM is also not as efficient as the FEM in simulating non-linear material behavior, such as plasticity and damage evolution processes, whereas is more suitable for solving problems of fracturing in homogeneous and linearly elastic bodies. The BEM formulation described above is called the direct formulation in which the displacements and tractions in the equations have clear physical meanings, are the basic unknowns of the boundary integral equations which are explicitly described on the problem boundary, and can be directly obtained by the solution of the integral equations. In the indirect formulation, on the other hand, the basic unknowns have no physical meanings and are just fictitious source densities related to the physical variables such as displacements and tractions. The typical indirect BEMs are the Displacement Discontinuity Method (DDM) by Crouch (1976) for 2D problems and Weaver (1977) for 3D problems. The basic concept of the indirect approach is to place the finite domain of interest into an imaginary infinitely large domain (full or half plane or spaces) to derive the boundary integral equations relating the physical variables, such as displacements and tractions, to fictitious source densities, such as fictitious load (stress) or displacement discontinuity.

A.4   Discontinuum methods

A.4.1   DISCRETE ELEMENT METHOD (DEM)

Rock mechanics is one of the disciplines from which the DEM originated (Cundall, 1971). The method has a broad variety of applications in rock mechanics, soil mechanics, structural analysis, granular materials, material processing, fluid mechanics, multi-body systems, etc. It is one of most rapidly developing areas of computational mechanics.

The DEM for modeling a discontinuum is relatively new compared with FDM, FEM and BEM and focuses mostly on applications in the fields of fractured or particulate geological media. The essence of the DEM is to represent the fractured medium as assemblages of blocks formed by connected fractures in the problem domain, and solve the equations of motion of these blocks through continuous detection and treatment of contacts between the blocks. The blocks can be rigid or be deformable with FDM or FEM discretizations. Large displacements caused by rigid body motion of individual blocks, including block rotation, fracture opening and complete detachments is straightforward in the DEM, but impossible in the FDM, FEM or BEM.

The theoretical foundation of the method is the formulation and solution of equations of motion of rigid and/or deformable bodies using implicit (based on FEM discretization) and explicit (using FVM discretization) formulations.

The key concept of DEM is that the domain of interest is treated as an assemblage of rigid or deformable blocks (particles, bodies) and the contacts among them need to be identified and continuously updated during the entire deformation/motion process, and represented by proper constitutive models.

To formulate a DEM method to simulate the mechanical processes in rock mechanics applications, the following problems must be solved:

1. space sub-division and identification of block system topology;

2. representation of block deformation (rigid or deformable, using FVM or FEM);

3. developing an algorithm for contact detection (penalty function, Lagrange multiplier, or augmented Lagrange multiplier);

4. obtaining constitutive equations for the rock blocks and fractures;

5. integration of the equations of motion of the blocks/particles (dynamic relaxation; time-marching FVM).

For rigid block analysis, an explicit time-marching scheme is used to solve the dynamic equations of motion of the rigid block system, based on a dynamic or static relaxation

scheme, or an FDM approach in the time domain. For deformable block systems, the solution strategies are different for the treatment of block deformability. One is explicit solution with finite volume discretization of the block interiors, without the need for solving large-scale matrix equations. The other is an implicit solution with finite element discretization of the block interiors, which leads to a matrix equation representing the deformability of the block systems, similar to that of the FEM.

The most representative *explicit DEM* methods is the Distinct Element Method created by (Cundall, 1980,1988) with the computer codes UDEC and 3DEC for 2D and 3D problems of rock mechanics (ITASCA Consulting Group, 1993c).

The *implicit DEM* was represented mainly by the Discontinuous Deformation Analysis (DDA) approach, originated by Shi (1988). The method uses standard FEM meshes over blocks and the contacts are treated using the penalty method. In terms of development and application, the DDA approach occupies the front position. DDA has two advantages over the explicit DEM: permission for relatively larger time steps and closed-form integrations for the stiffness matrices of elements. An existing FEM code can also be readily transformed into a DDA code while keeping all the advantageous features of the FEM.

Another similar development, called the combined finite-DEM (Munjiza et al., 1995; Munjiza and Andrews, 2000), considers not only the block deformation but also fracturing and fragmentation of the rocks.

A.4.2   Explicit DEM - Distinct Element Method

The Distinct Element Method was originated in the early 70s by a landmark paper on the progressive movements of rock masses as 2D rigid block assemblages (Cundall, 1971). The technique of the explicit DEM is presented comprehensively in Cundall and Hart (1992).

A.4.2.1   Block discretization

Blocks are represented as convex polyhedra in 3D with each face a planar convex polygon having a finite number of rectilinear edges. Their 2D counterparts are general polygons with a finite number of straight edges (Figure A.2). The 2D polygons can be either convex or concave, but the 3D polyhedral must be convex. These blocks are formed by fractures which are represented in the problem domain either individually (for larger-scale fractures) or by a fracture sets generator (for smaller-scale fracture sets) using random distributions (based on site or modeling requirement data) of dip angles, dip directions, spacing and apertures of the sets. The vertices (corners), edges and faces of
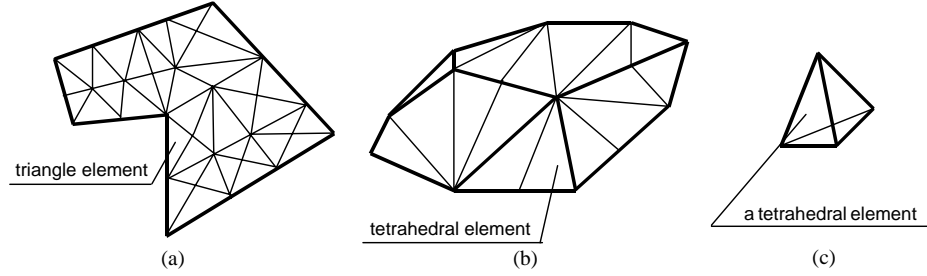
Figure A.2: Discretization of blocks by: (a) constant strain triangles; (b) constant strain tetrahedral; and (c) a typical tetrahedral element (Jing, 2003).

individual blocks and their connection relations are identified during the block generation process. The deformable blocks are further divided into a finite number of constant strain triangles in 2D or tetrahedra in 3D. These triangles or tetrahedra form a mesh of the FVM (zones). Rectangular element meshes can also be used for 2D problems when the problem geometry is favorable.

A.4.2.2   Representation of deformation

An explicit, large strain Lagrangian formulation for the constant strain elements is used to represent the element deformations. The displacement field of each element varies linearly and the faces or edges of the elements remain as planar surface or straight line segments. Higher order elements may also be used, but curved boundary surfaces (or edges) may be obtained, which may in turn complicate the contact-detection algorithm. Based on Gauss' theorem to convert volume (area) integrals into surface (line) integrals, the increments of element strain can be written

$$\Delta \varepsilon_{ij} \approx \frac{\Delta t}{2} \sum_{k=1}^{N} \left[(v_i^m)\, n_j \pm \left(v_j^m\right) n_i \right] \Delta S^k \tag{A.16}$$

where ΔS^k is the area (or length) of the kth boundary face (or edge) with unit normal n_i^k, and v_i^m is the mean value of velocity over ΔS^k. The summation extends over the N faces (or edges) of an element (zone). The sign "+" is used if $i + j$; otherwise, the sign "-" is used. Δt is the time step. The stress increments are obtained by invoking the constitutive equations for the block materials.

A.4.2.3 Representation of contacts

Kinematically, block contacts are determined by the smallest distance between two blocks, pre-set in the codes or models. When this distance is within a prescribed threshold, a potential contact between these two blocks is numerically established. The contact-detection algorithm in the Distinct Element Method programs determines the contact type (different touching patterns between vertices, edges and faces), the maximum gap (if two blocks do not touch but are separated by a gap close to the pre-set tolerance), and the unit normal vector defining the tangential plane on which sliding can take place.

Table A.1 lists all types of contacts. Mechanically, the interaction between two contacting blocks is characterized by a stiffness (spring) in the normal direction and a stiffness and friction angle (spring-slip surface series) in the tangential directions with respect to the fracture surface (contact plane, see Figure A.3a).

Block shapes	Contact types
Arbitrary polygons (convex or concave) (2-D block)	vertex-to-vertex, vertex-to-edge, edge-to-edge
Convex polyhedral (3D block)	vertex-to-vertex, vertex-to-edge, vertex-to-face, edge-to-edge, edge-to-face, face-to-face

Table A.1: Types of contacts for polygons and polyhedral.

Interaction forces developed at contact points are determined as linear or non-linear functions of the deformations of springs and slip surfaces (i.e., the relative movements of blocks at contact points) and resolved into normal and tangential components, depending the constitutive models of the contacts (point contacts or edge/face contacts). The concept of contact "overlap", though physically inadmissible in block kinematics (because blocks should not interpenetrate each other) may be accepted as a mathematical means to represent the deformability of the contacts. However, it does present a numerical shortcoming that is difficult to overcome when the normal forces or stresses at contact points are large. In this case, even with high normal stiffness, the "overlap" may be too excessive to be acceptable and the calculation has to be stopped to implement some remedial measure (for example, to increase the normal stiffness) and start again. It also presents a problem for fluid flow calculation in which the apertures of fractures may become negative if "overlap" occurs at contact points. The mathematical representation of the contact "overlap" is thus not fully compatible with physical reality.
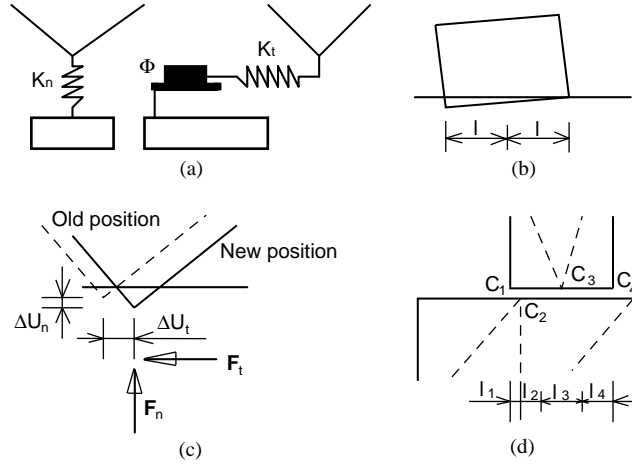
Figure A.3: Mechanical representation of contacts in the 2D DEM (Jing, 2003).

A.4.2.4 Numerical integration of equations of motion

An explicit central difference scheme is applied in the Distinct Element Method to integrate the equations of motion of the block system, as opposed to the implicit approach utilized in other continuum based numerical methods. The unknown variables (contact forces or stresses) on the block boundary or in the internal elements are determined locally at each time step from the known variables on the boundaries, in the elements and their immediate neighbors. There is no need to set up and solve a matrix form of the equations of motion. The non-linearity in the material behavior (of the fractures or intact blocks) can be handled in a straightforward manner.

The equations of motion for a rigid block, in terms of translational and rotational velocities, are written

$$v_i^{(t+\Delta t/2)} = v_i^{(t-\Delta t/2)} + \left[\frac{\sum f_i}{m} + b_i \right] \Delta t$$

$$\omega_i^{(t+\Delta t/2)} = \omega_i^{(t-\Delta t/2)} + \frac{\sum M_i}{I} \Delta t \tag{A.17}$$

where m is the block mass, I is the moment of inertia, b_i are the volume force components of the block and M_i are the components of the resultant moment. The displacement at

the next time step is then given by

$$u_i^{(t+\Delta t)} = u_i^{(t)} + v_i^{(t+\Delta t/2)}\Delta t$$
$$\theta_i^{(t+\Delta t)} = \theta_i^{(t)} + \omega_i^{(t+\Delta t/2)}\Delta t \tag{A.18}$$

where θ_i is the angular displacement of the block.

For deformable blocks, the equations of motion are written for grid points - the vertices of internal difference elements. The central difference scheme is similar to the first equation in Equation A.17 with only one modification to the resultant out-of-balance force, f_i

$$f_i = f_i^C + \sum_{k=1}^{N} \sigma_{ij}\left(n_j^k\Delta S^k\right) \tag{A.19}$$

where f_c^i is the resultant contact force if the grid point is on the boundary of the block. The symbol N denotes the number of difference elements connected by this grid point. At each time step, the kinematic quantities (velocities, displacements and accelerations) are first calculated and the contact forces or stresses, as well as the internal stresses of the elements, are then obtained via constitutive relations for contacts. In the general calculation procedure, two basic tasks are performed in turn. The kinematic quantities are updated first, followed by invoking the constitutive relations to provide the corresponding forces and stresses.

A.4.2.5 Applications

Due to the explicit representation of fractures, the DEM, especially the Distinct Element Method, hase been widely applicated in rock engineering. The applications of DEM concentrate on hard rock problems and have increasing focus on coupled hydro-mechanical behavior - because of the dominating effects of the rock fractures on these aspects, and so where the explicit representation of fractures is necessary (Sharma et al., 2001). For the softer and weaker rocks, equivalent continuum models are more applicable because there is less difference between the deformability of the fractures and the rock matrix.

Despite the advantages of DEM, lack of knowledge of the geometry of the rock fractures limits its more general applications. In general, the geometry of fracture systems in rock masses cannot be known and can only be roughly estimated. The adequacy of the DEM results in capturing the rock reality are therefore highly dependent on the interpretation of the in situ fracture system geometry - which cannot be even moderately validated in practice. Of course, the same problem applies also to the continuum models,

such as the FEM or FDM, but the requirement for explicit fracture geometry representation in the DEM highlights the limitation and makes it more acute. Monte Carlo fracture simulation may help to reduce the level of uncertainty, with increased computation cost.

A.4.3 Implicit DEM - Discontinuum Deformation Analysis method

DDA originated from a back analysis algorithm for determining a best fit to a deformed configuration of a block system from measured displacements and deformations (Shi and Goodman, 1985). It was later further developed to perform complete deformation analysis of a block system (Shi, 1988).

By the second law of thermodynamics, a mechanical system under loading (external and/or internal) must move or deform in a direction which produces the minimum total energy of the whole system. For a block system, the total energy consists of the potential energy due to different mechanisms like external loads, block deformation, system constraints, kinetic and strain energy of the blocks and the dissipated irreversible energy. The minimization of the system energy will produce an equation of motion for the block system, the same as that used in the FEM. For a system of N blocks, each having m_i nodes $(i = 1, 2, ..., N)$, the total number of nodes is $m_1 + m_2 + ... + m_N = M$, and each node has two orthogonal displacement variables, u and v. Assuming, without losing generality, that nodes are numbered sequentially blockwise, the minimization will yield $(2M \times 2M)$ simultaneous equations, written symbolically as

$$
\begin{bmatrix}
\mathbf{k}_{11} & \mathbf{k}_{12} & \mathbf{k}_{13} & \dots & \mathbf{k}_{1N} \\
\mathbf{k}_{21} & \mathbf{k}_{22} & \mathbf{k}_{23} & \dots & \mathbf{k}_{2N} \\
\mathbf{k}_{31} & \mathbf{k}_{32} & \mathbf{k}_{33} & \dots & \mathbf{k}_{3N} \\
\vdots & \vdots & \vdots & \vdots & \vdots \\
\mathbf{k}_{N1} & \mathbf{k}_{N2} & \mathbf{k}_{N3} & \dots & \mathbf{k}_{NN}
\end{bmatrix}
\begin{Bmatrix}
\mathbf{d}_1 \\ \mathbf{d}_2 \\ \mathbf{d}_3 \\ \vdots \\ \mathbf{d}_N
\end{Bmatrix}
=
\begin{Bmatrix}
\mathbf{f}_1 \\ \mathbf{f}_2 \\ \mathbf{f}_3 \\ \vdots \\ \mathbf{f}_N
\end{Bmatrix}
\quad or \ [\mathbf{K}]\,\{\mathbf{D}\} = \{\mathbf{F}\} \quad \text{(A.20)}
$$

where diagonal sub-matrices $\mathbf{k}_{ij}$ is a $(2m_i \times 2m_i)$ matrix representing the sum of contributing sub-matrices for the ith block of m_i nodes. Vector $\mathbf{d}_i$ is a $(2m_i \times 1)$ vector of displacement variables of the ith block and vector $\mathbf{f}_i$ is a $(2m_i \times 1)$ vector of resultant general forces acting on the ith block. The off-diagonal sub-matrices $\mathbf{k}_{ij}$ $(i \neq j)$ represent the sum of contributing sub-matrices of contacts between blocks i and j and other inter-block actions like bolting. The matrix $[\mathbf{K}]$ can also be called the global "stiffness matrix".

Compared with the explicit approach of the DEM, the DDA method has four basic advantages over the explicit DEM:

1. the equilibrium condition is automatically satisfied for quasi-static problems without using excessive iteration cycles;

2. the length of the time step can be larger, and without inducing numerical instability;

3. closed-form integrations for the element and block stiffness matrices can be performed without the need for Gaussian quadrature techniques;

4. it is easy to convert an existing FEM code into a DDA code and include many mature FEM techniques without inheriting the limitations of the ordinary FEM, such as small deformation, continuous material geometry, and reduced efficiency for dynamic analysis. However, matrix equations are produced and need to be solved, using the same FEM technique.

The DDA method has emerged as an attractive model for geomechanical problems because its advantages cannot be replaced by continuum-based methods or explicit DEM formulations.

A.4.4   DISCRETE FRACTURE NETWORK (DFN) method

The DFN method is a special discrete model that considers fluid flow and transport processes in fractured rock masses through a system of connected fractures. The DFN model is established on the understanding and representation of the two key factors: fracture system geometry and transmissivity of individual fractures.

The stochastic simulation of fracture systems is the geometric basis of the DFN approach and plays a crucial role in the performance and reliability of the DFN model, in the same way as the DEM. The key process is to create PDFs of fracture parameters relating to the densities, orientations and sizes, based on field mapping results using borehole logging data and scan line or window mapping techniques, and generate the realizations of the fractures systems according to these PDFs and assumptions about fracture shape (circular discs, ellipses or polygons), (Dershowitz, 1984; Billaux et al., 1989).

Numerical techniques have been developed for the solution of flow fields for individual fracture elements using closed-form solutions, the finite element model, the boundary element model, the pipe model and the channel lattice model.

Closed-form solutions exist, at present, only for planar, smooth fractures with parallel surfaces of regular shape (i.e. circular or rectangular discs) for steady-state flow (Long, 1983) or for both steady state and transient flow (Amadei and Illangasekare, 1992). For fractures with general shapes, numerical solutions must be used. The FEM discretization technique is perhaps the most well-known techniques used in the DFN flow models and
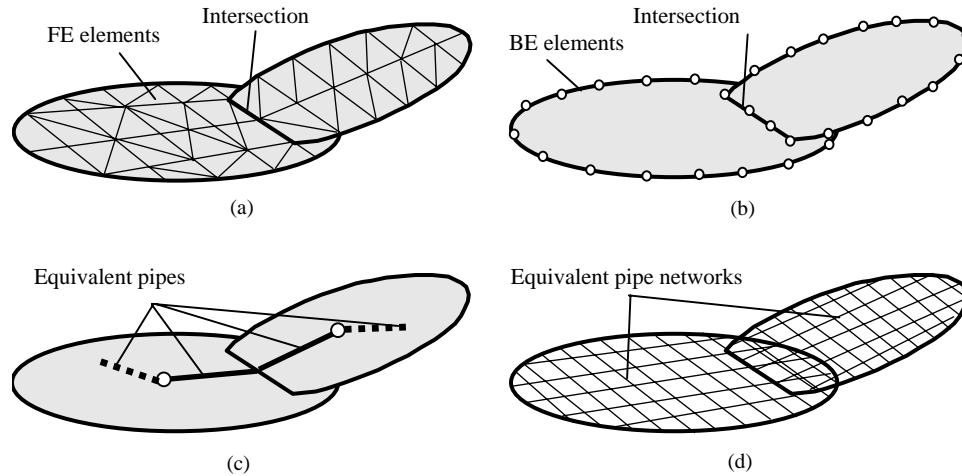
Figure A.4: Representation of rock fractures for the flow equation solution: (a) FEM; (b) BEM; (c) equivalent pipes; and (d) channel lattice model (Jing, 2003).

has been used in the DFN codes FRACMAN/MAFIC (Dershowitz et al., 1993) and NAP-SAC (Herbert, 1994). The basic concept is to impose a FEM mesh over the individual discs representing fractures in space (Figure A.4a) and solve the flow equations. The aperture or transmissivity field within the fracture can be either constant or randomly distributed. Similarly, the BEM discretization can also be applied with the boundary elements defined only on the disc boundaries (Figure A.4b), with the fracture intersections treated as internal boundaries in the BEM solution. The compatibility condition is imposed at the intersections of discs.

The pipe model represents a fracture as a pipe of equivalent hydraulic conductivity starting at the disc center and ending at the intersections with other fractures (Figure A.4c), based on the fracture transmissivity, size and shape distributions.

The channel lattice model represents the whole fracture by a network of regular pipe networks (Figure A.4d). The pipe model leads to a simpler representation of the fracture system geometry, but may have difficulties to properly represent systems of a number of large fractures. The channel lattice model is more suitable for simulating the complex flow behavior inside the fracturesand is computationally less demanding than the FEM and BEM models since the solutions of the flow fields through the pipe elements are analytical.

A.5   Hybrid models

Hybrid models are frequently used in rock engineering, basically for flow and stress-deformation problems of fractured rocks. The main types of hybrid models are the hybrid BEM/FEM and DEM/BEM models. The hybrid DEM/FEM models are also developed. The BEM is most commonly used for simulating far-field rocks as an equivalent elastic continuum, and the FEM and DEM for the non-linear or fractured near-field where explicit representation of fractures or non-linear mechanical behavior, such as plasticity, is needed. This harmonizes the geometry of the required problem resolution with the numerical techniques available, thus providing an effective representation of the effects of the far-field to the near-field rocks.

A.5.1   HYBRID FEM/BEM MODELS

The hybrid FEM/BEM was first proposed in Zienkiewicz et al. (1977) as a general stress analysis technique. The standard technique is to treat the BEM region as a "super" element with an artificially "symmetrized" stiffness matrix, using the least-square techniques, so that it can be easily inserted into the symmetric FEM stiffness matrix for the final solution, which is easier to handle than the non-symmetric BEM stiffness matrix. However, such artificial "symmetrization" introduces additional errors into the final system equations. The coupling can also be performed in the opposite direction, i.e. treat the FEM region as a "super" BEM element, and insert the corresponding FEM stiffness matrix into the final BEM stiffness matrix; this leads to a asymmetric stiffness matrix for the final equation, which needs additional computational efforts for solution.

The hybrid BEM/FEM models are as efficient computationally as the FEM, with the additional advantage of being able to deal with the non-linear behavior of materials in the FEM region, using the FEM's advantages. However, this advantage may be affected by the symmetrized BEM equation. A possible step forward in this direction is to use the Galerkin double integration techniques in the BEM region so that the final BEM stiffness matrix is automatically symmetric, and therefore can be directly inserted in the final hybrid BEM/FEM matrix without errors caused by artificial "symmetrization".

A.5.2   HYBRID DEM/BEM MODELS

The hybrid DEM/BEM model was implemented only for the explicit Distinct Element Method, in the code group of UDEC and 3DEC. The technique was created by Lorig and Brady (1982), and was implemented into UDEC by Lemos (1987). The basic concept is to treat the BEM region (which surrounds the DEM region) as a "super" block having con-
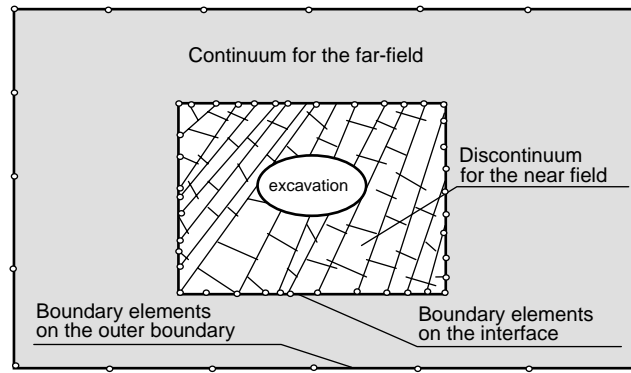
Figure A.5: Hybrid model for a rock mass containing an excavation-using the DEM for the near-field region close to the excavation and the BEM for the far-field region (Jing, 2003).

tacts with smaller blocks along the interfaces with the DEM region (Figure A.5), which can be treated in standard DEM contact representations. The key conditions are:

1. the kinematic continuity along the interfaces of the two regions during the time-marching process;

2. the elastic properties of the two regions near the interface are similar.

Condition 2 indicates that blocks in the DEM regions must be deformable, i.e. not be rigid blocks. In the case of mixed rigid and deformable block systems, special equations of motion need to be developed to handle such cases.

A.5.3   Hybrid FEM/DEM models

Besides the above mainstream hybrid formulations, there are other coupling techniques which take advantage of different numerical methods. Pan and Reed (1991) reported a hybrid DEM/FEM model, in which the DEM region consists of rigid blocks and the FEM region can have non-linear material behavior. The algorithm places the FEM calculations into the DEM time-marching process. Since the blocks in DEM region are rigid and the FEM region is an elastic continuum, the kinematical continuity condition along the interface of the DEM and FEM regions may not be satisfied.

The hybrid FEM/DEM model has been recently implemented in ELFEN, a commercial numerical code developed by Rockfield (Swansea, UK), since 1986. The development has been undertaken collaboration with the Institute of Numerical Methods in Engineering (INME) at University of Wales Swansea, which is internationally well-known for its pioneering work in this area. ELFEN is a dynamic solver based on the Finite Element Method (FEM) and specialized in problems of transition from a continuum to a discontinuum material. It includes specific non linear fracture mechanics algorithms to simulate the fracturing and produce discrete fractures (Klerck et al., 2004). If the fracture criterion within the intact rock (represented by FEM) is met, then a crack (represented by DEM) is initiated. Adaptive re-meshing allows the fracture process through the FEM mesh to be tracked and visualized; thus contact properties can be assigned to pre-existing cracks and newly generated cracks.

A.6 Numerical modeling of fracture process

Modeling fractured rocks demands high performance numerical methods and computer codes, especially regarding fracture representations, material heterogeneity and non-linearity, coupling with fluid flow and heat transfer and scale effects.

It is often restrictive to use only one method to provide adequate representations for the most significant features and processes: hybrid models or multiple process codes are often used in combination. There are no absolute advantages of one method over another. However, some of the disadvantages inherent in one type can be avoided by combined continuum-discrete models, termed hybrid models.

A.6.1 Fracture analysis with FDM/FVM

Explicit representation of fractures is not easy in FDM/FVM because the finite difference schemes in FDM and interpolations in FVM require continuity of the functions between the neighboring grid points. During the early development of FVM approaches, it is possible to represent weakness zones of certain thickness as collections of cells of different materials, which are not permitted to have openings or to be detached from their neighboring cells. The FDM/FVM deformable models have been used to study the mechanisms of macroscopic fracturing processes, such as shear-band formation in the laboratory testing of rock and soil samples and slope stability. This is achieved as a process of material failure or damage propagation at the grid points or cell centers, without creating fracture surfaces in the models.

A.6.2   Fracture analyses with FEM

Representation of rock fractures in the FEM has been motivated by rock mechanics needs since the late 1960s, with the most notably contributions from Goodman et al. (1968), Zienkiewicz et al. (1970), Ghaboussi et al. (1973), Katona (1983), Desai et al. (1984).

Assuming that the contact stresses and relative displacements along and across the rock fractures of a theoretical zero thickness (Figure A.6a), Goodman et al. (1968) proposed a "joint element" which can be readily incorporated into an FEM process.

The well-known "Goodman joint element" in rock mechanics literature, has been widely implemented in FEM codes and applied to many practical rock engineering problems. Also, it has been extended to consider peak and post-peak behavior in the shear direction. However, its formulation is based on continuum assumptions, so that large-scale opening, sliding, and complete detachment of elements are not permitted. Because of the zero thickness of the joint element, numerical ill-conditioning may arise due to large aspect ratios (the ratio of length to thickness) of joint elements.

Zienkiewicz et al. (1970) proposed a six-node fracture element with two additional nodes in the middle section of the element, and a small thickness (Figure A.6c). The elements can, therefore, be curved. The formulation may be seen as a "degenerate" ordinary solid element of narrow thickness, and is subject to numerical ill-conditioning when the aspect ratio is too large.

Using the relative displacements between the two opposite surfaces of fractures as the independent system unknowns, Ghaboussi et al. (1973) proposed an FEM joint element based on the theory of plasticity (Figure A.6b). The use of the relative displacement components across and along the fractures of finite thickness reduces the number of unknowns of the fracture elements by half, defined at two nodes instead of four nodes as in Goodman's joint elements. A finite thickness t is also used. The normal and shear strain components of the element are defined as the corresponding ratios of relative normal and shear displacements over the fracture thickness. An elasto-plastic relation between the normal and shear stresses and the normal and shear strains of the fracture element is formulated and can be implemented in the usual manner for continuum FEM analysis. This formulation is more robust in terms of numerical ill-conditioning as compared with those proposed in Goodman et al. (1968) and Zienkiewicz et al. (1970), due to the use of the relative displacements.

The "thin-layer" elements developed by Desai et al. (1984) are also based on a continuum assumption; these are a solid element with a specially developed constitutive model for contact and frictional sliding.

The fracture element formulation in FEM has also been developed with interface element models in contact mechanics, using the FEM approach, instead of the continuum solid element approximation as mentioned above. Katona (1983) developed an FEM in-
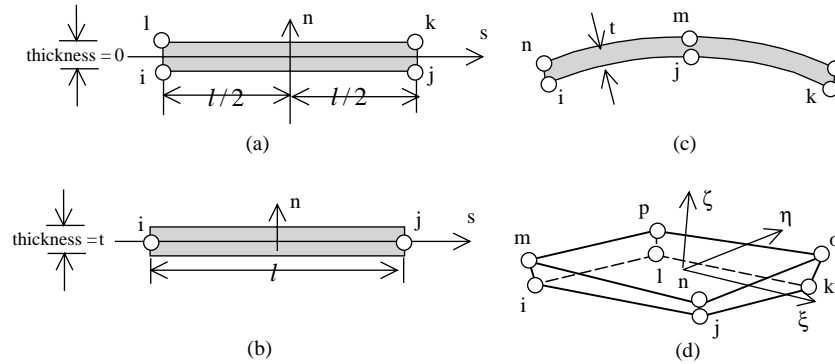
Figure A.6: Fracture elements in FEM by (a) Goodman et al. (1968), (b) Ghaboussi et al. (1973), (c) Zienkiewicz et al. (1970) and (d) Buczkowski and Kleiber (1997).

terface element model defined by mating pairs of nodes, without using the normal and shear stiffness parameters, and with three states - sticking, slipping and opening - based on the Coulomb friction law.

Despite these efforts, the treatment of fractures and fracture growth remains the most important limiting factor in the application of the FEM for rock mechanics problems, especially when large number of fractures needs to be represented explicitly. The FEM suffers from the fact that the global stiffness matrix tends to be ill-conditioned when many fracture elements are incorporated. Block rotations, complete detachment and large-scale fracture opening cannot be treated because the general continuum assumption in FEM formulations requires that fracture elements cannot be torn apart.

However, special algorithms have been developed in an attempt to overcome this disadvantage, e.g. using discontinuous shape functions (Wan, 1990) for implicit simulation of fracture initiation and growth through bifurcation theory.

A special class of FEM, often called "enriched FEM", has been especially developed for fracture analysis with minimal or no re-meshing, as reported in Belytschko and Black (1999). The basic concept is direct representation of the objective function (such as displacements) with arbitrary discontinuities and discontinuous derivatives in FEM, but without need for the FEM meshes to conform to the fractures and no need for re-meshing for fracture growth.

The treatment of fractures is at the element level. The surfaces of the fractures are defined by assigned distance functions so that their representation requires only nodal function values, represented by an additional degree of freedom in the trial functions, a
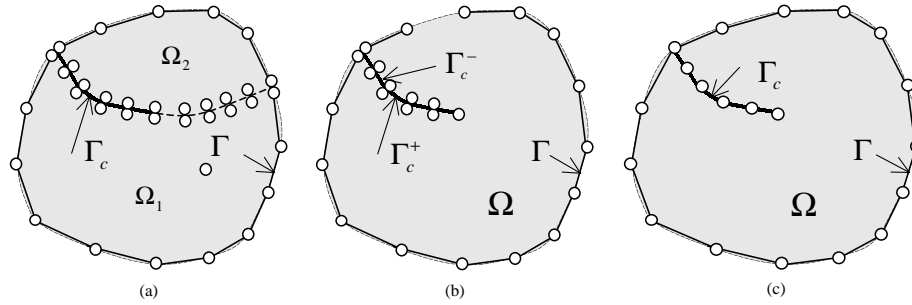
Figure A.7: Illustrative meshes for fracture analysis with BEM: (a) sub-domain, direct BEM; (b) single domain, dual BEM; and (c) single domain DDM (Jing, 2003).

jump function along the fracture and a crack tip function at the tips. In Belytschko et al. (2001), the enriched method was applied to a tunnel stability analysis with fractures simulated as displacement discontinuities.

The "enriched" FEM with jump functions and crack tip functions has improved the FEM's capacity in fracture analysis. Coupled with the FEM's advantage in dealing with material heterogeneity and non-linearity, this makes the "enriched" FEM suitable for non-linear fracture analysis. One such example is the so-called "generalized finite element method" (GFEM), which was developed based on the partition of unity principle (Duarte et al., 2000). The mesh in GFEM is independent of the geometry of the domain of interest and therefore can be regular regardless of the object geometry. Fractures can be simulated by their surrounding nodes "enriched" by jump functions and crack tip functions.

A.6.3   Fracture analyses with BEM

To apply standard direct BEM for fracture analysis, the fractures must be assumed to have two opposite surfaces, except at the apex of the fracture tip where special singular tip elements must be used.

Because of the very small thickness of fractures, the two nodes at the opposite surfaces of a fracture will in fact occupy the same coordinates. This will naturally lead to singular global stiffness matrices if the same boundary conditions (or unknowns) are specified at the two opposite fracture surfaces.

To overcome these difficulties, two techniques were proposed. One was to divide the problem domain into multiple sub-domains with fractures along their interfaces (Figure A.7a), by Blandford et al. (1981). This way, the stiffness matrices contributed by opposite surfaces of the same fracture will belong to different sub-domain stiffness matrices; thus, the singularity of the global matrix is avoided. This technique, however, requires the knowledge of fracturing paths (used for deciding sub-regions) and growth rate (for deciding element sizes), which is determined by the solution of the problem itself, before the problem solution, and may not be applicable for many practical problems without symmetry in geometry and boundary conditions.

The second technique is the Dual Boundary Element Method (DBEM) (Portela, 1992). The essence of this technique is to apply displacement boundary equations at one surface of a fracture element and traction boundary equations at its opposite surface, although the two opposing surfaces occupy practically the same space in the model. The general mixed mode fracture analysis can be performed naturally in a single domain (Figure A.7b). The original concept of using two independent boundary integral equations for fracture analysis, one displacement equation and another its normal derivative, was developed first by Watson (1979).

The DDM has been widely applied to simulate fracturing processes in fracture mechanics in general and in rock fracture propagation problems in particular due to the advantage that the fractures can be represented by single fracture elements without need for separate representation of their two opposite surfaces, as should be done in the direct BEM solutions. It was developed by Crouch and Starfield (1983) with open fractures, and was extended to fractures with contact and friction by Shen (1991) for rock engineering analyses.

References

Amadei, B. and Illangasekare, T. (**1992**). "Analytical solutions for steady and transient flow in non-homogeneous and anisotropic rock joints." *International Journal of Rock Mechanics and Mining Science and Geomechanics Abstracts*, 29(6): 561–572.

Beer, G. and Meek, J. L. (**1981**). "Infinite domain elements." *International Journal for Numerical Methods in Engineering*, 17(1): 43–52.

Belytschko, T. and Black, T. (**1999**). "Elastic crack growth in finite elements with minimal remeshing." *International Journal for Numerical Methods in Engineering*, 45(5): 601–620.

Belytschko, T., Moës, N., Usui, S., and Parimi, C. (**2001**). "Arbitrary discontinuities in finite elements." *International Journal for Numerical Methods in Engineering*, 50(4): 993–1013.

Billaux, D., Chiles, J. P., Hestir, K., and Long, J. C. S. (**1989**). "Three-dimensional statistical modeling of a fractured rock mass-an example from the Fanay-Augéres Mine." *International Journal of Rock Mechanics and Mining Science and Geomechanics Abstracts*, 26(3-4): 281–299.

Blandford, G., Ingraffea, A., and Liggett, J. (**1981**). "Two-dimensional stress intensity factor computations using the boundary element method." *International Journal for Numerical Methods in Engineering*, 17(3): 387–404.

Brighi, B., Chipot, M., and Gut, E. (**1998**). "Finite differences on triangular grids." *Numerical Methods for Partial Differential Equations*, 14(5): 567–579.

Buczkowski, R. and Kleiber, M. (**1997**). "Elasto-plastic interface model for 3D-frictional orthotropic contact problems." *International Journal for Numerical Methods in Engineering*, 40(4): 599–619.

Crouch, S. and Starfield, A. (**1983**). *Boundary element methods in solid mechanics*. George Allen and Unwin.

Crouch, S. L. (**1976**). "Solution of plane elasticity problems by the displacement discontinuity method. I. Infinite body solution." *International Journal for Numerical Methods in Engineering*, 10(2): 301–343.

Cundall, P. A. (**1971**). "A computer model for simulating progressive large scale movements in blocky rock systems." In "Proceedings of International Symposium on Rock Fracture," volume 2. ISRM, Nancy.

Cundall, P. A. (**1980**). "UDEC - a generalized distinct element program for modelling jointed rock." Technical Report Report PCAR-l-80, Peter Cundall Associates, European Research Office, US Army Corps of Engineers.

Cundall, P. A. (**1988**). "Formulation of a three-dimensional distinct element model-Part I. A scheme to detect and represent contacts in a system composed of many polyhedral blocks." *Int. J. Rock Mech. Min. Sci. and Geomech.*, 25(3): 107–116.

Cundall, P. A. and Hart, R. D. (**1992**). "Numerical modelling of discontinua." *Engineering Computations*, 9(2): 101–113.

Dershowitz, W. S. (**1984**). *Rock joint systems*. Ph.D. thesis, Massachusetts Institute of Technology, Boston, USA.

Dershowitz, W. S., Lee, G., Geier, J., Hitchcock, S., and La Pointe, P. (**1993**). *FracMan user documentation*. Golder Associates Inc., Seattle WA.

Desai, C. S., Zaman, M. M., Lightner, J. G., and Siriwardane, H. J. (**1984**). "Thin-layer element for interfaces and joints." *International Journal for Numerical and Analytical Methods in Geomechanics*, 8(1): 19–43.

Duarte, C. A., Babuska, I., and Oden, J. T. (**2000**). "Generalized finite element methods for three-dimensional structural mechanics problems." *Computers and Structures*, 77(2): 215–232.

Ghaboussi, J., Wilson, E. L., and Isenberg, J. (**1973**). "Finite element for rock joints and interfaces." *Journal of the Soil Mechanics and Foundations Division ASCE*, 99(10): 849–862.

Goodman, R., Taylor, R., and Brekke, T. (**1968**). "A model for the mechanics of jointed rock." *J Soil Mech Div ASCE*, 94(SM3): 637–659.

Herbert, A. (**1994**). *NAPSAC (Release 3.0) summary document*. AEA Technology, Harwell, UK.

ITASCA Consulting Group, L. (**1993**b). *FLAC manuals*.

ITASCA Consulting Group, L. (**1993**c). *UDEC manuals*.

Jing, L. (**2003**). "A review of techniques, advances and outstanding issues in numerical modelling for rock mechanics and rock engineering." *International Journal of Rock Mechanics and Mining Sciences*, 40(3): 283–353.

Katona, M. (**1983**). "A simple contact-friction interface element with applications to buried culverts." *International Journal for Numerical and Analytical Methods in Geomechanics*, 7(3): 371–384.

Klerck, P. A., Sellers, E. J., and Owen, D. R. J. (**2004**). "Discrete fracture in quasi-brittle materials under compressive and tensile stress states." *Computer Methods in Applied Mechanics and Engineering*, 193(27-29): 3035–3056.

Lemos, J. V. (**1987**). *A hybrid distinct element computational model for the half-plane*. Master's thesis, Department of Civil Engineering, University of Minnesota.

Long, J. C. S. (**1983**). *Investigation of equivalent porous media permeability in networks of discontinuous fractures*. Ph.D. thesis, Lawrence Berkeley Laboratory, University of California, Berkeley, CA.

Lorig, L. J. and Brady, B. H. G. (**1982**). "A hybrid discrete element-boundary element method of stress analysis." In R. E. Goodman and F. Heuze, editors, "Proceedings of the 23rd US Symposium Rock Mechanics, Berkeley," pages 628–636.

Munjiza, A. and Andrews, K. R. F. (**2000**). "Penalty function method for combined finite-discrete element systems comprising large number of separate bodies." *International Journal for Numerical Methods in Engineering*, 49(11): 1377–1396.

Munjiza, A., Owen, D. R. J., and Bicanic, N. (**1995**). "A combined finite-discrete element method in transient dynamics of fracturing solids." *Engineering Computations*, 12(2): 145–174.

Pan, X. and Reed, M. (**1991**). "A coupled distinct element-finite element method for large deformation analysis of rock masses." *International Journal of Rock Mechanics and Mining Science & Geomechanics Abstracts*, 28(1): 93–99.

Perrone, N. and Kao, R. (**1975**). "A general finite difference method for arbitrary meshes." *Computers and Structures*, 5: 45–58.

Portela, A. (**1992**). *Dual boundary element incremental analysis of crack growth.* Ph.D. thesis, Wessex Institute of Technology, Portsmouth University, Southampton, UK.

Sharma, V., Saxena, K., and Woods, R. (**2001**). *Distinct element modelling in geomechanics.* Balkema, Rotterdam.

Shen, B. (**1991**). *Mechanics of fractures and intervening bridges in hard rocks.* Ph.D. thesis, Royal Institute of Technology, Stockholm, Sweden.

Shi, G. (**1988**). *Discontinuous deformation analysis-a new numerical model for the statics, dynamics of block systems.* Ph.D. thesis, University of California, Berkeley, USA.

Shi, G. H. and Goodman, R. E. (**1985**). "Two dimensional discontinuous deformation analysis." *International Journal for Numerical and Analytical Methods in Geomechanics*, 9(6): 541–556.

Wan, R. (**1990**). *The numerical modeling of shear bands in geological materials.* Ph.D. thesis, University of Alberta, Edmonton, AB.

Watson, J. O. (**1979**). "Advanced implementation of the boundary element method for two- and three-dimensional elastostatics." In P. K. Banerjee and R. Butterfield, editors, "Developments in boundary element methods, vol. 1," pages 31–63. Applied Science Publishers, London.

Weaver, J. (**1977**). "Three-dimensional crack analysis." *International Journal of Solids and Structures*, 13(4): 321–330.

Wheel, M. A. (**1996**). "A geometrically versatile finite volume formulation for plane elastostatic stress analysis." *The Journal of Strain Analysis for Engineering Design*, 31(2): 111–116.

Zienkiewicz, O., Emson, C., and Bettess, P. (**1983**). "A novel boundary infinite element." *International Journal for Numerical Methods in Engineering*, 19(3): 393–404.

Zienkiewicz, O., Kelly, D., and Bettess, P. (**1977**). "The coupling of the finite element method and boundary solution procedures." *International Journal for Numerical Methods in Engineering*, 11(2): 355–375.

Zienkiewicz, O. C., Best, B., Dullage, C., and Stagg, K. (**1970**). "Analysis of non-linear problems in rock mechanics with particular reference to jointed rock systems." In "Proceedings of the 2nd International Congress on Rock Mechanics, ISRM, Belgrade," .

Appendix B

Rock anisotropy

B.1 Introduction

In this appendix the attention is posed on rock anisotropy. A review of the deformability and strength anisotropy is done, in order to introduce the numerical modelling of some of the most common laboratory tests carried out on anisotropic rocks.

B.2 The nature of rock masses

The nature of rock masses is complex and resulting from a long history of tectonic forces and other natural environmental effects.

In the context of continuum mechanics, the material and the forces applied to it have to be considered. In rock mechanics, there is the intact rock divided by discontinuities to form the rock structure which is subjected to the *in situ* stress and influenced by factors such as water flow and time. In all these subjects the geological history has played its part, altering the rock and the applied forces.

In engineering terms, *intact rock* is defined as rock without significant fractures. The most complete description of the behaviour of intact rock is the complete stress-strain curve obtained in a uniaxial compression test (Figure B.1). The uniaxial compression test is conducted by loading a sample of rock along its axis and recording the displacement produced as the force is increased. From the stress-strain curve it is possible to define three important parameters. The first one is the Young's modulus, E, defined as the ratio of stress to strain, and the second one is the maximum stress that the specimen can sus-

tain. Under the loading conditions shown in the diagram, the peak stress is the uniaxial compressive strength, σ_c. A third interesting feature is the steepness of the descending portion of the curve, that is a measure of rock brittleness.
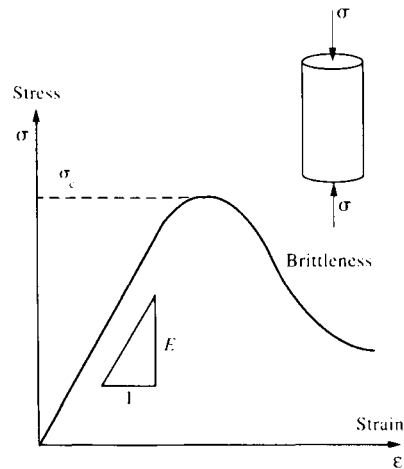
Figure B.1: The complete stress-strain curve illustrating various mechanical parameters (Hudson and Harrison, 1997).

During the history of the rock mass, due to the action of geological and environmental factors, the rock does break and the result is a complex structure of fractures forming rock blocks. The overall geometrical configuration of the discontinuities in the rock mass is termed *rock structure*.

It is helpful to understand how the fractures form: there are three modes of fracture, illustrated in Figure B.2. These types of fracture lead to two fundamentally different type of discontinuities:

- joints, discontinuity that has been simply opened;

- shear zone or faults, discontinuity which has been subjected to some lateral movements.

Such features exist in all rock masses and they will significantly affect the deformability, strength and failure of rock masses. Other key characteristics, such as the permeability can be governed almost entirely by the rock structure configuration.
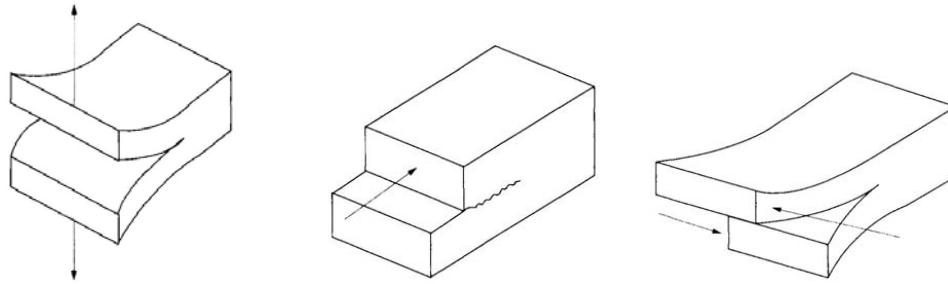
Figure B.2: Type of fracturing in rock: mode I - tensile; mode II - in plane shear; mode III - out of plane shear (Hudson and Harrison, 1997).

In this way, the deformation, strength and failure properties of a *rock structure* are determined by the mechanical properties of the intact rock and the geometrical and the mechanical properties of the natural fractures of the rock mass.

B.3   Definitions

When dealing with the mechanical behaviour of solids, a common assumption is that they are homogeneous, continuous and isotropic, but the mechanical properties of rock mass are, however, not at all isotropic. In fact, rock mass anisotropy and inhomogeneity are two important aspects to take into account when rock engineering problems are considered. Such characteristics are a natural consequence of millions of years of mechanical, chemical and thermal processes to which the rock mass has been subjected.

The term "anisotropy" means "having different properties in different directions", whereas the word "inhomogeneity" means "having different properties at different locations". In rock mechanics, these properties may be of any type: deformability, strength, brittleness, permeability and discontinuity frequency.

In the context of rock engineering, the anisotropic and inhomogeneous behaviour is explained using two acronyms, CHILE and DIANE (Harrison and Hudson, 2000):

- Continuous, Homogeneous, Isotropic and Linearly-Elastic (CHILE) material is one that is most commonly assumed for the purpose of modelling; traditionally stress

analysis techniques are formulated in terms of these four attributes, simply for convenience for obtaining closed-form solutions;

- Discontinuous, Inhomogeneous, Anisotropic, Non-Elastic (DIANE) rock is the material with which the rock engineering has to deal.

The rock is *discontinuous* because of the bedding plane separations and any other fracturing that may be present. It is *inhomogeneous* because of the existence of the different rock type. It is *anisotropic* because of its sedimentary nature. It is *not elastic* because there is hysteresis and time dependency, related to bedding planes. Moreover, the rock is anisotropic because it is inhomogeneous, e.g. the deformation modulus for a suite of strata will be different parallel and perpendicular of the bedding planes. Also, the rock is anisotropic because it is discontinuous.

B.4   Deformability anisotropy

There are three types of isotropy commonly considered in rock mechanics: complete isotropy, transverse isotropy and orthotropy. As indicated by the sketches in Figure B.3, transverse isotropy might well represent relatively unfractured sedimentary rocks, whereas, orthotropy could well be a good representation for rocks containing three mutually perpendicular sets of discontinuity.

In order to define the compliance matrix, it is assumed that each component of the strain tensor is a linear combination of all the components of the stress tensor. In the case of the ε_{xx} component, the relation is expressed as

$$\varepsilon_{xx} = S_{11}\sigma_{xx} + S_{12}\sigma_{yy} + S_{13}\sigma_{zz} + S_{14}\tau_{xy} + S_{15}\tau_{yz} + S_{16}\tau_{zx}$$

Because there are six independent components of the strain matrix, there will be six equations of this type. If it is considered that the strain in the x-direction were only due to the stress in the x-direction, the previous equation would reduce to

$$\varepsilon_{xx} = S_{11}\sigma_{xx}$$

or

$$\sigma_{xx} = \varepsilon_{xx}/S_{11} = E\varepsilon_{xx}$$

where $E = 1/S_{11}$.

Isotropic   Transversely isotropic (horizontal)   Orthotropic

$$\sigma_x = \sigma_y = \left(\frac{\nu}{1-\nu} \right) \sigma_z \qquad \sigma_x = \sigma_y = \left(\frac{\nu_{xz}}{1-\nu} \right) \sigma_z \qquad \sigma_x = \left(\frac{\nu_{xz} + \nu_{yz}\,\nu_{xy}}{1 - \nu_{xy}\,\nu_{yx}} \right) \sigma_z$$

$$\nu = \nu_{xy} = \nu_{xz} = \nu_{yz} \qquad\qquad \nu_{xy} = \nu_{yx} = \nu \qquad\qquad \sigma_y = \left(\frac{\nu_{yz} + \nu_{yx}\,\nu_{xz}}{1 - \nu_{xy}\,\nu_{yx}} \right) \sigma_z$$
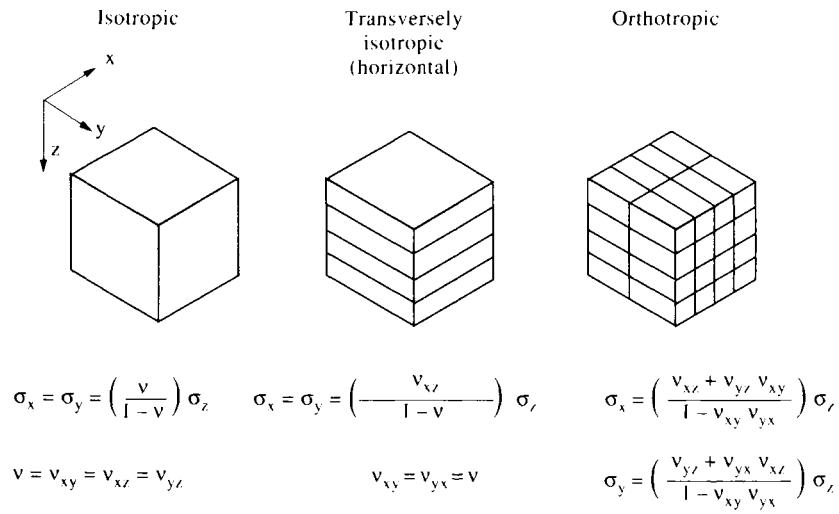
Figure B.3: Relation between vertical and elastically induced horizontal stresses for the different type of isotropy (from Hudson and Harrison, 1997).

The complete set of relations between the strain tensor and stress components written in matrix notation is:

$$|\varepsilon| = |S||\sigma|$$

where

$$
[\varepsilon] =
\begin{bmatrix}
\varepsilon_{xx} \\
\varepsilon_{yy} \\
\varepsilon_{zz} \\
\varepsilon_{xy} \\
\varepsilon_{yz} \\
\varepsilon_{zx}
\end{bmatrix}
\quad \text{and} \quad
[\sigma] =
\begin{bmatrix}
\sigma_{xx} \\
\sigma_{yy} \\
\sigma_{zz} \\
\sigma_{xy} \\
\sigma_{yz} \\
\sigma_{zx}
\end{bmatrix}
\quad \text{and} \quad
[S] =
\begin{bmatrix}
S_{11} & S_{12} & S_{13} & S_{14} & S_{15} & S_{16} \\
 & S_{22} & S_{23} & S_{24} & S_{25} & S_{26} \\
 & & S_{33} & S_{34} & S_{35} & S_{36} \\
 & & & S_{44} & S_{45} & S_{46} \\
 & & & & S_{55} & S_{56} \\
 & & & & & S_{66}
\end{bmatrix}
$$

The $[S]$ matrix shown above is known as the **compliance matrix**. In general the higher the magnitude of a specific element in this matrix, the greater will be the contribution to the strain. "Compliance" is a form of "flexibility", and it is the inverse of "stiffness". The compliance matrix is a 6 x 6 matrix containing 36 elements and it is symmetrical. In order to define the matrix it is necessary to define 21 independent elastic constants to completely characterize a material that follows the generalized Hooke's law.

An **orthotropic material** is characterized by 9 independent elastic constants which are three Young's moduli and the three shear moduli and the three Poisson's ratio, i.e.:

$$E_1 \; E_2 \; E_3 \; G_{12} \; G_{23} \; G_{31} \; v_{21} \; v_{32} \; v_{31}$$

The compliance matrix could be reduced even further considering the case of **transverse isotropy**. This is represented by a rock mass with a laminated fabric or one set of parallel discontinuities. In the case when the plane of isotropy is parallel to the plane containing Cartesian axes 1 and 2, it is possible to say that:

$$E_1 = E_2 = E \quad \text{and} \quad E_3 = E'$$

$$v_{12} = v_{21} = v \quad \text{and} \quad v_{13} = v_{23} = v'$$

$$G_{12} \neq G_{23} \quad \text{and} \quad G_{23} = G_{31} = G'$$

The associated compliance matrix is then

$$
\begin{bmatrix}
1/E & \frac{-v}{E} & \frac{-v'}{E} & 0 & 0 & 0 \\
 & 1/E & \frac{-v'}{E} & 0 & 0 & 0 \\
 & & 1/E' & 0 & 0 & 0 \\
 & & & \frac{2(1+v)}{E} & 0 & 0 \\
 & & & & 1/G' & 0 \\
sym. & & & & & 1/G'
\end{bmatrix}
$$
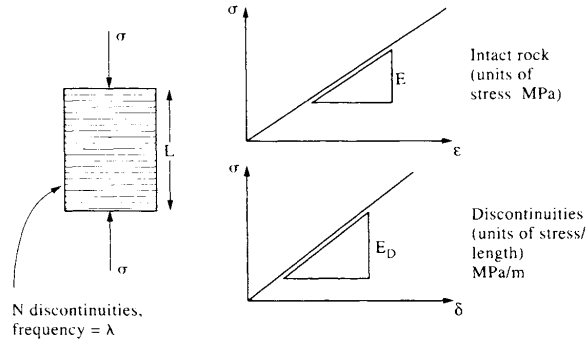
Figure B.4: The modulus of deformation of a rock mass containing a discontinuity set (Hudson and Harrison, 1997).

note that the term $2(1 + v)/E$ has been substituted for $1/G_{12}$ because in the plane of isotropy there is a relation between the shear modulus G and the Young's modulus E and Poisson's ratio v. Thus the number of independent elastic constants for a transversely isotropic material is 5:

$$E_1 \; E' \; G' v \; v'$$

The final reduction can be made to the compliance matrix of a **completely isotropic** material, resulting in 2 elastic constants (also using the shear modulus relation):

$$E_1 = E_2 = E_3 = E$$

$$v_{12} = v_{23} = v_{31} = v$$

$$G_{12} = G_{23} = G_{31} = G$$

Now the attention is posed on the rock mass in order to provide a model for the deformability (Hudson and Harrison, 1997). Consider first, the deformation of a set of parallel discontinuities under the action of a normal stress, assuming linear elastic discontinuity stiffnesses. This circumstance is illustrated in figure B.4.

To calculate the overall modulus of deformation, the applied stress is divided by the total deformation. The deformation is made up of two components: one due to the deformation of the intact rock; the other due to the deformability of the discontinuities. In this calculation, the assumption that the thickness of the discontinuities is negligible in comparison to the overall length, L, is taken. The contribution made by the intact rock to

the deformation, δ_I, is $\sigma L / E$ (i.e. strain multiplied by length). The contribution made by a single discontinuity to the deformation, δ_D, is σ / E_D (E_D relates the stress to displacement directly). Assuming a discontinuity frequency of λ, there will be λL discontinuities in the rock mass and the total contribution made by these to the deformation will be δ_D^t, which is equal to $\sigma \lambda L / E_D$. Hence, the total displacement, δ_T, is

$$\delta_T = \frac{\sigma L}{E} + \frac{\lambda \sigma L}{E_D}$$

with the overall strain being given by

$$\varepsilon = \frac{\delta_t}{L} = \frac{\sigma}{E} + \frac{\lambda \sigma}{E_D}$$

Finally, the overall modulus, E_{MASS}, is given by

$$E_{MASS} = \frac{\sigma}{\varepsilon} = \frac{1}{\frac{1}{E} + \frac{\lambda}{E_D}}$$

$$G_{MASS} = \frac{\tau}{\gamma} = \frac{1}{\frac{1}{G} + \frac{\lambda}{G_D}}$$

B.5   Strength anisotropy

In the same way as it has been considered the deformability of a rock mass, expressions can be developed indicating how strength is affected by the presence of discontinuities, starting with a single discontinuity and then extending to any number of discontinuities (Hudson and Harrison, 1997).

The strength of a sample of intact rock containing a single discontinuity can be established using the "single plane weakness" theory (Jaeger, 1960). Basically, the stress applied to the sample is resolved into the normal and shear stresses on the plane of weakness and the Mohr-Coulomb failure criterion applied to consider the possibility of slip. The strength of the sample depends on the orientation of the discontinuity. If the discontinuity is, for example, parallel or perpendicular to the applied loading, it will have no effect on the sample strength. At some angles, however, the discontinuity will significantly reduce the strength of the sample. This is illustrate in Figure B.5 which shows that the lowest strength occurs when the discontinuity normal is inclined at an angle of $45° + (\phi_w / 2)$ to the major applied principal stress.

The formula for the reduction in strength is found by establishing the normal and shear stress on the plane passing through the specimen and substituting these into the
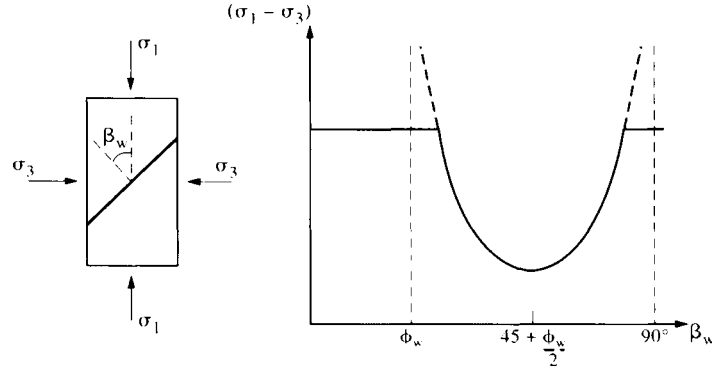
Figure B.5: Effect of a discontinuity on the strength of a rock sample according with Mohr-Coulomb criterion (Hudson and Harrison, 1997).

Mohr-Coulomb failure criterion. Given the geometry of the applied loading conditions in Figure B.5,

$$|\tau| = \frac{1}{2} \left(\sigma_1 - \sigma_3\right) \sin 2\beta_w$$

$$\sigma_n = \frac{1}{2} \left(\sigma_1 + \sigma_3\right) + \frac{1}{2} \left(\sigma_1 - \sigma_3\right) \cos 2\beta_w$$

Substituting these into the Mohr-Coulomb criterion, $|\tau_n| = c_w + \sigma_n \tan \phi_w$, and rearranging,

$$\left(\sigma_1 - \sigma_3\right) = \frac{2 \left(c_w + \sigma_3 \tan \phi_w\right)}{\left(1 - \cot \beta_w \tan \phi_w\right) \sin 2\beta_w}$$

where c_w and ϕ_w are the cohesion and the angle of friction for the discontinuity (i.e. plane of weakness), and β_w is illustrated in Figure B.5. The plot of the equation in figure B.5 shows the minimum strength and also the angles at which the sample strength becomes less than that of the intact rock. Outside of the region, failure occurs more easily on a plane other than the plane of weakness: the failure occurs at Mohr-Coulomb stress and the predicted failure plane is oriented at 45°-($\phi_w/2$), independently of the orientation of the plane of weakness.
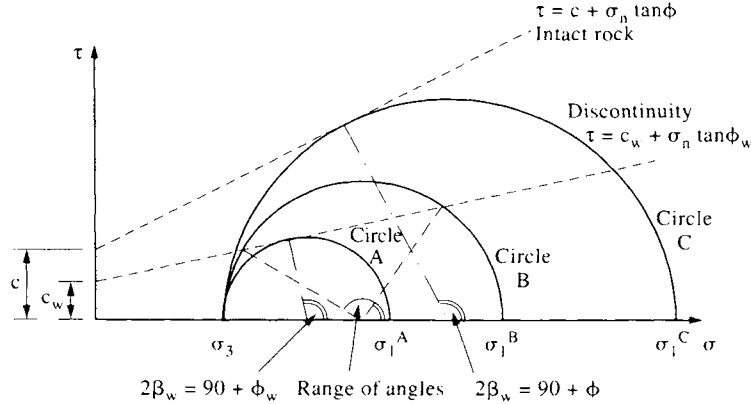
Figure B.6: Mohr's circle representation of the possible modes of failure for rock containing a single plane of weakness (Harrison and Hudson, 2000).

An alternative presentation is via the Mohr's circle representation, as shown in Figure B.6. The Mohr-Coulomb failure loci for both the intact rock and the discontinuity are shown. It is also shown three Mohr's circle, A, B and C, representing the lowest strength, an intermediate case and the highest strength.

- Circle A represents the case when the failure locus for the discontinuity is just reached, i.e. for a discontinuity at the angle $2\beta_w = 90° + \phi_w$.

- Circle B is a case when failure can occur along the discontinuity for a range of angles, as indicated in figure.

- Circle C represents the case where the circle touches the intact rock failure locus, i.e. where the failure will occur in the intact rock if it has not already done so along the discontinuity.

Relations identical to the above have been derived from the equivalent Griffith crack model in which it is assumed that there are two population of cracks, long cracks lying parallel to a given plane, the plane of weakness, and short cracks randomly oriented, and the cracks are closed and subjected to friction in the relative sliding of their surfaces (Paterson and Wong, 2005).

It is possible to consider, on the basis of the single plane of weakness theory, what would happen if there were two or more discontinuities at different orientations present
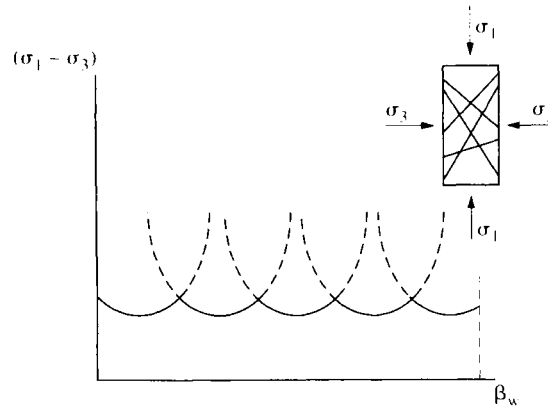
Figure B.7: Strength of a rock mass containing multiple discontinuity sets (Harrison and Hudson, 2000).

in the rock sample (Hudson and Harrison, 1997). Each discontinuity would weaken the sample as indicated in Figure B.7, but the angular position of the strength would not coincide. As a result the rock is weakened in several different directions simultaneously (Figure B.7). The material tends to become isotropic in strength, like a granular soil. When plotting the superimposed curves, care should be taken in interpreting the magnitude of β_w correctly for each of the discontinuities concerned.

Figure B.8 demonstrates the anisotropy of compressive strength recorded for a series of test performed on a slate (Hudson and Harrison, 1997). This is an example of anisotropy characterised through application of the single plane of weakness theory, which have directionally built into its formulation.
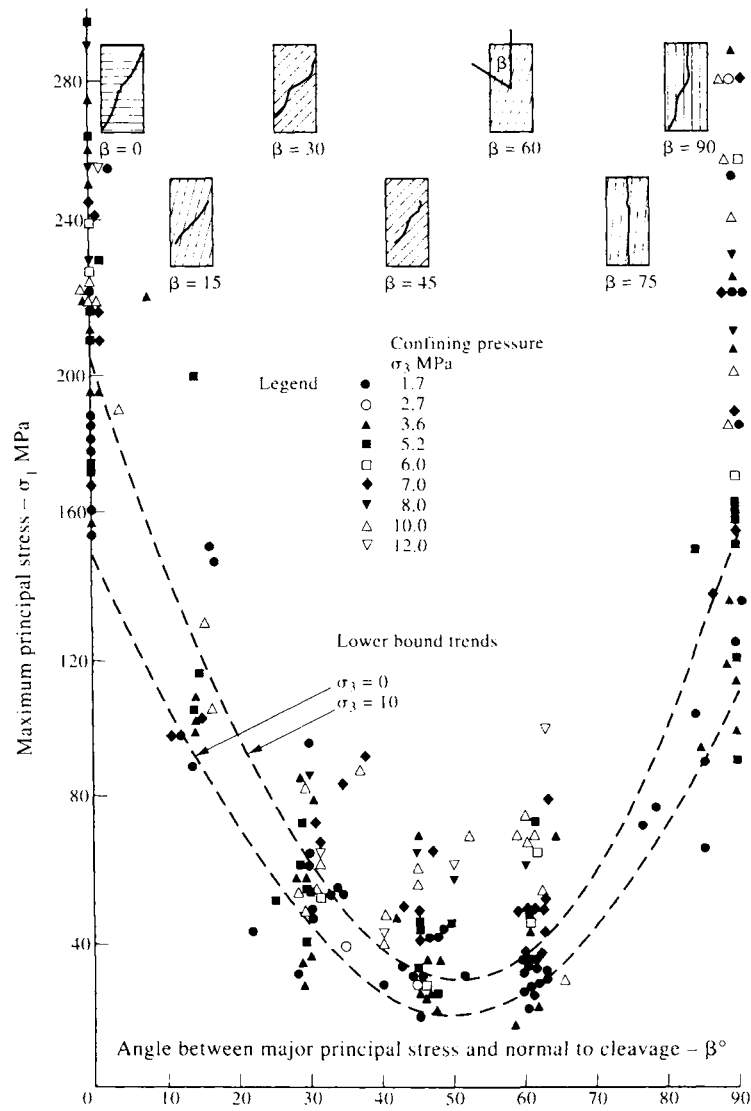
Figure B.8: Anisotropy of compressive strength in slate rock (Harrison and Hudson, 2000).

B.6   Numerical modelling of anisotropic rock

Starting from the CHILE and DIANE assumptions, it will be helpful to consider aniso-tropy and inhomogeneity in the modelling procedures. According to the circumstances, failure can either occur along the discontinuities or through the intact rock, depending on the relative orientations of the principal stresses and the discontinuities.

When the rock mass initially reaches its peak strength due to the application of stresses, either the intact rock or a fracture will begin to fail. Hence, the properties that govern the failure of rock masses are the failure properties of the intact rock and the fractures. The orientation of the applied stresses relative to the fractures governs how failure occurs, bearing in mind that the failure of a rock mass is a complex structural breakdown process following a similar curve to that in Figure B.1 for the intact rock.

The development of computer based numerical solutions helps to deal with more complex geometry and material properties. These techniques include finite difference, finite element, boundary element and distinct element formulations, providing the capability of incorporating discontinuousness, anisotropy, inhomogeneity and more complex constitutive behaviour.

All the numerical techniques can accommodate wide variations in problem geometry and the presence of discontinuities. This is not the case for the inhomogeneity, aniso-tropy and constitutive behaviour relating to volume properties, because the individual elements in these numerical formulations should not be assigned a single value relating to a volume property which may varying on a scale commensurate with the elements themselves. Developments aimed at overcoming these difficulties are the use of hybrid numerical formulations which recognize the advantages of the continuum and discontinuum component methods.

B.7   FDEM modelling of laboratory tests on anisotropic rock

The scope of this study is to simulate the behaviour of a layered rock specimen under a standard laboratory test. Data collected from uniaxial and triaxial laboratory tests of Luserna gneiss (Barla et al., 1989) and Martinsburg slate (Donath, 1964) were compared with numerical results obtained using the Y2D code. Note that, in the following numerical analyses, only strength anisotropy will be analysed because the Y2D code takes no account of the deformability anisotropy.

B.7.1 Numerical modelling of uniaxial tests of gneiss

The rock specimen to be considered is a cylinder of 54 mm in diameter with a ratio height/diameter of 2.5:1. In a uniaxial test, the specimens are loaded axially up to failure whereby the specimen is deformed and the axial and the radial deformation can be measured.

Several numerical simulations have been carried out by considering uniaxial compression tests of Luserna Gneiss specimens obtained from a site in Northwest Alps, in Italy (Barla et al., 1989). Each specimen was characterised by a different angle between the direction of loading and the orientation of the joints planes. The spacing between the joints was 30 mm (Figure B.9).
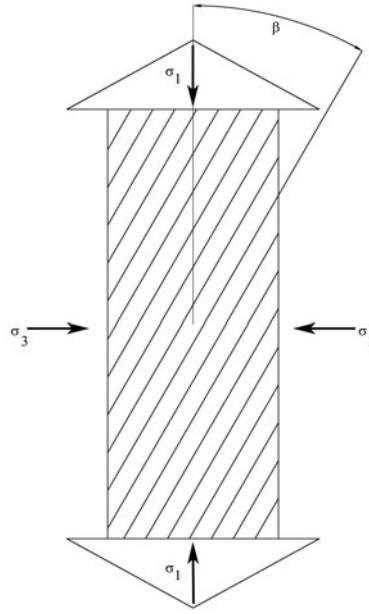
Figure B.9: Schematic of the rock specimen; σ_1 is the axial stress, σ_3 is the confining pressure and β is the inclination of joints.

The properties of intact rock and joints are shown in Table B.1. A Mohr-Coulomb material with maximum tensile strength cut-off was used both for intact rock and joints.

	Rock sample	Joints	Loading platens
Elastic modulus, E (GPa)	30	-	193
Poisson's Ratio, ν (-)	0.3	-	0.29
Density, ρ (kg/m^3)	2700	-	8030
Internal cohesion, c_i (MPa)	18.30	13.97	-
Internal friction angle, ϕ_i (°)	59.52	48.43	-
Tensile strength, σ_i (MPa)	17	4	-
Fracture energy release rate, G_f (J/m^2)	200	50	-

Table B.1: Material properties of gneiss, joints and loading platens.

An unstructured mesh with average element size of 1 mm was generated with Phase^2 and used in numerical analysis with the Y2D code. Figure B.10 shows the geometry (load, mesh and joints) of the seven specimens analysed.

To simulate a uniaxial test, a constant vertical velocity (0.25 mm/s) was applied to the loading platens. Usually, in laboratory tests a quasi-static displacement rate (e.g. 0.01mm/s) is applied. Considering the size of the time-step needed to satisfy the stability condition of the explicit time integration scheme, a simulation which reproduces the velocity applied in a laboratory test would have resulted in a very long computation time. Tests carried out on the velocity applied to the loading platens demonstrate that a peak strength convergent to the quasi-static condition value can been obtained by using a relatively high displacement rate (i.e. 0.25 mm/s). During the simulation, the reaction force at the nodes of the upper and lower platens, the vertical stress, the y-displacement of a point of the specimen next to the platens, and the x-displacement of the lateral boundary of the sample have been recorded.

The stress-strain curves obtained from numerical modelling of uniaxial tests on gneiss are plotted in Figure B.11. Table B.2 compares the values of the uniaxial compressive strength obtained from laboratory tests, numerical modelling, and the theoretical values according to Mohr-Coulomb criterion (modified). This comparison is plotted on Figure B.12.

The effect of anisotropy on rock strength can be considered according to the theoretical model described in the first part of this appendix. As shown in Figure B.12 the lowest strength occurs when the discontinuity normal is inclined at an angle of 45°-($\phi_w/2$) (i.e. 20.78°) to the major applied principal stress.

The fracture pattern obtained in the numerical modelling with the Y2D code, when the joints are vertical (i.e $\beta=0°$) is shown in Figure B.13. Fractures develop along the bedding planes first, then shear bands form. The splitting process can be considered
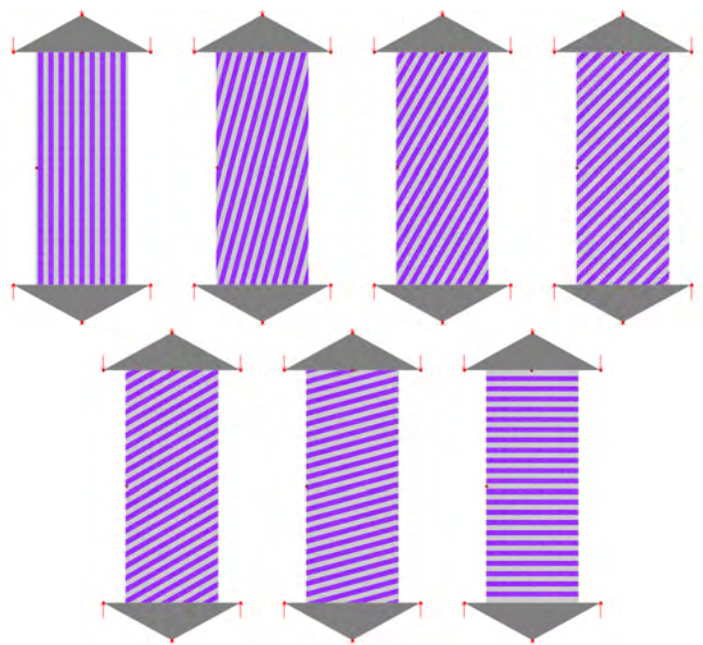
Figure B.10: Jointed specimens of Luserna gneiss: geometry and mesh.

	0°	15°	30°	45°	60°	75°	90°
UX laboratory test	116.21	101.68	92.46	75.68	116.68	127.96	152.44
Mohr-Coulomb	134	80	92	134	134	134	134
Numerical	134	72	126	112	111	112	111

Table B.2: Comparison among laboratory, numerical and theoretical values of compressive strength from uniaxial test of Luserna gneiss.
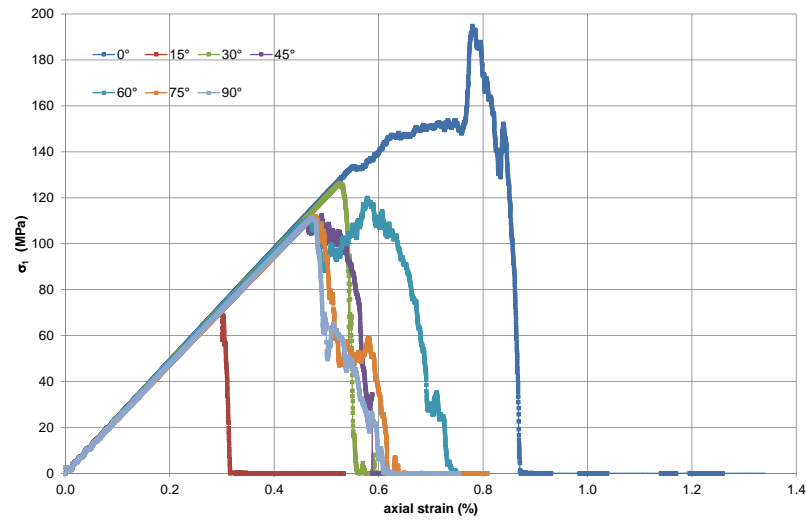
Figure B.11: Uniaxial tests of Luserna gneiss: stress-strain curve for specimens characterised by a different inclination of joints (β). The curves have been obtained from the Y2D numerical modelling of uniaxial tests.
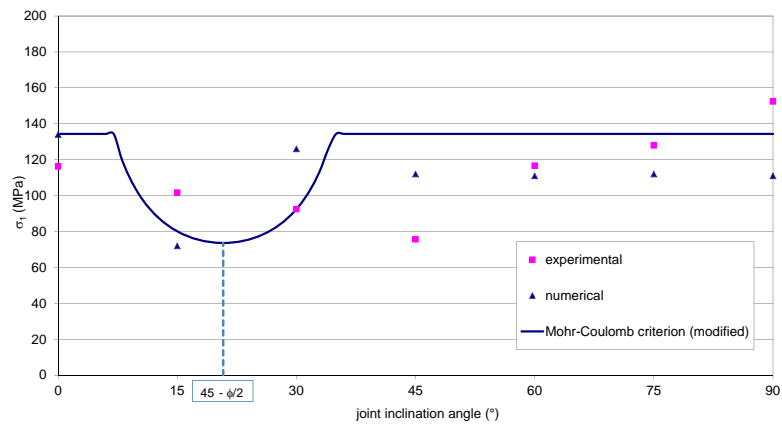
Figure B.12: Influence of anisotropy on rock strength (uniaxial tests of Luserna gneiss): comparison among numerical, theoretical and laboratory data.

predominant. For the sample with $\beta=15°$, it was found that pure shear fractures develop along the bedding planes (Figure B.14), whereas when the fracture are horizontal ($\beta=90°$), inclined shear fractures are observed (Figure B.15).
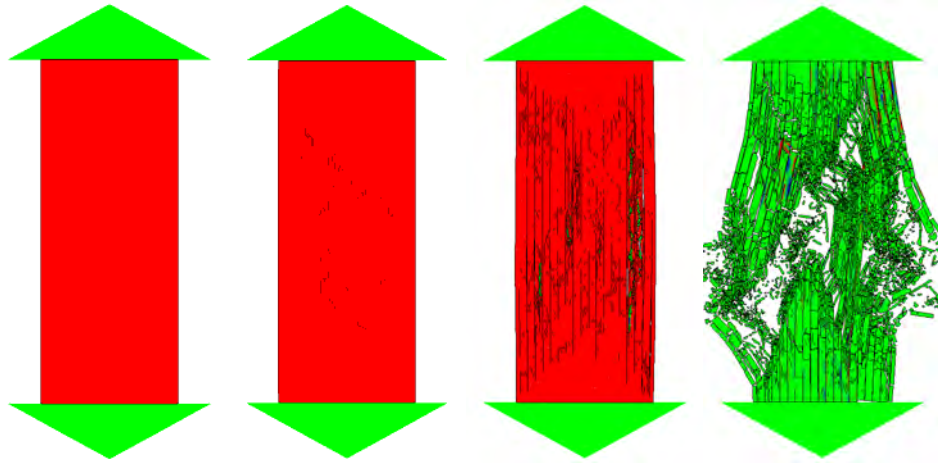
Figure B.13: Uniaxial test of a Luserna gneiss specimen ($\beta=0°$): fracture patterns simulated with the Y2D code. Colours represent vertical stresses (red: compressive).
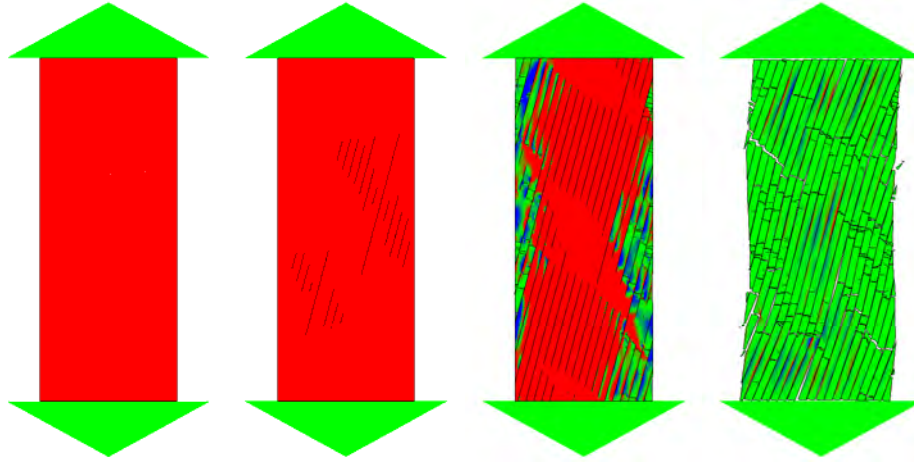
Figure B.14: Uniaxial test of a Luserna gneiss specimen (β=15°): fracture patterns simulated with the Y2D code. Colours represent vertical stresses (red: compressive).
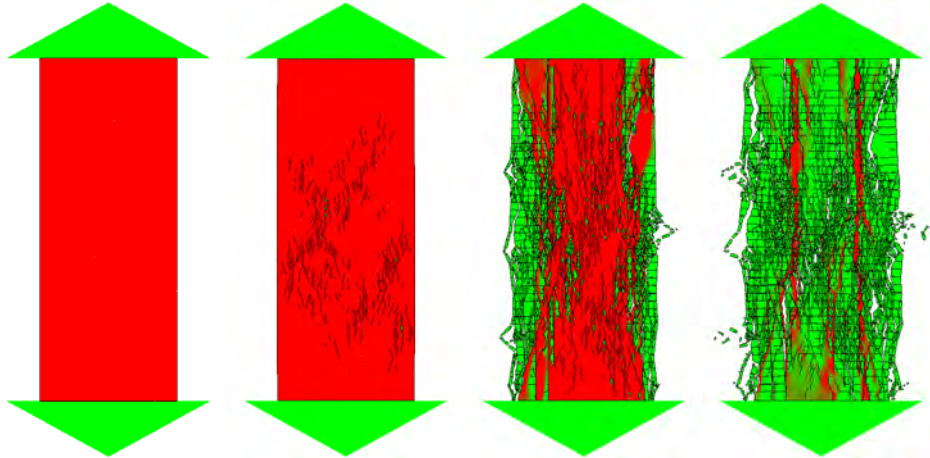
Figure B.15: Uniaxial test of a Luserna gneiss specimen (β=90°): fracture patterns simulated with the Y2D code. Colours represent vertical stresses (red: compressive).

B.7.2   Numerical modelling of uniaxial and triaxial tests of slate

The specimens under investigation is a rock cylinder of 54 mm in diameter with a ratio height/diameter of 2.5:1 for uniaxial test, and of 2:1 for triaxial test. In this numerical study, each rock specimen has been characterised by joints with a different inclination. Actually, the angle between the direction of loading and the orientation of the joints has been varied from 0° to 90° with an increment of 15°. The spacing between the joints planes is 30 mm.

The properties of intact rock and joints are listed in Table B.3. The intact rock and the joints behave according to the Mohr-Coulomb criterion with a maximum tensile strength cut-off. Each specimen was discretised with an unstructured mesh characterised by average element size of 1 mm. The mesh was generated in Phase², then imported in Y2D code. A triaxial test has been simulated for each rock specimen shown in Figure B.16, whereas the uniaxial tests have been simulated for rock specimen with the same geometry used in the numerical study on gneiss (Figure B.10). The boundary conditions applied to the loading platens are a constant vertical velocity of 0.25 mm/s and, in the triaxial tests, a confinement pressure of 10.5 MPa.

	Rock sample	Joints	Loading platens
Elastic modulus, E (GPa)	30	-	193
Poisson's Ratio, ν (-)	0.3	-	0.29
Density, ρ (kg/m^3)	2600	-	8030
Internal cohesion, c_i (MPa)	38.34	7.33	-
Internal friction angle, ϕ_i (°)	37.84	20.18	-
Tensile strength, σ_i (MPa)	19	1	-
Fracture energy release rate, G_f (J/m^2)	200	50	-

Table B.3: Material properties of Martinsburg slate, joints and loading platens.

The stress-strain curves resulting from the simulation of uniaxial tests and triaxial tests with the Y2D code are shown respectively in Figure B.17 and Figure B.18, whereas the values obtained from laboratory tests and numerical analyses are indicated in Table B.4. Using a confinement pressure, the peak load increases, and also the residual value after the peak increases.

As described in the first part of this appendix, the effect of anisotropy on rock strength can be considered with the relationships based on the Mohr Coulomb strength criterion, modified to take into account the presence of joints. The strength of the specimen depends on the orientation of the principal stresses relative to fracture orientation. Assum-
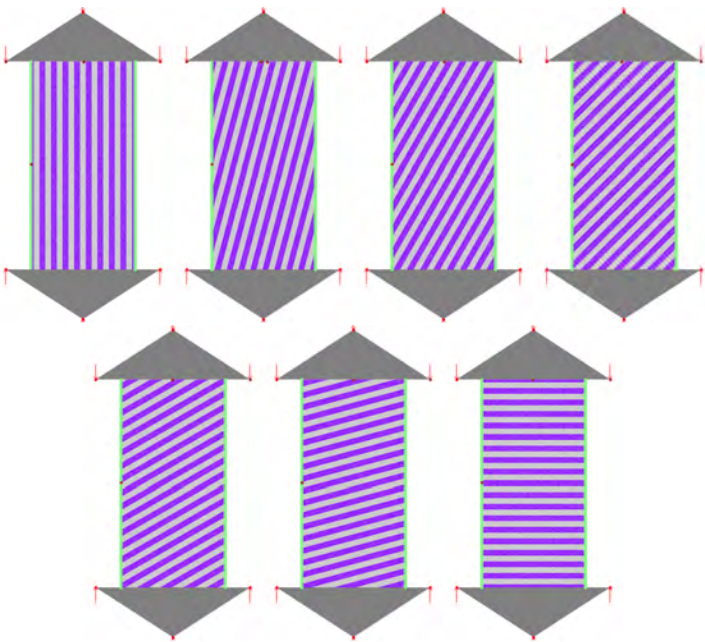
Figure B.16: Triaxial tests of Martinsburg slate. Multiple jointed specimens: mesh and joints orientation.

	0°	15°	30°	45°	60°	75°	90°
Mohr-Coulomb	157	33	21	23	47	157	157
Numerical	163	31	24	43	147	130	149
TX laboratory test	169	79	45	53	103	164	250
Mohr-Coulomb	200	60	43	46	85	200	200
Numerical	222	76	62	99	183	192	192

Table B.4: Comparison among laboratory, numerical and theoretical values of compressive strength from uniaxial tests and triaxial tests of Martinsburg slate.
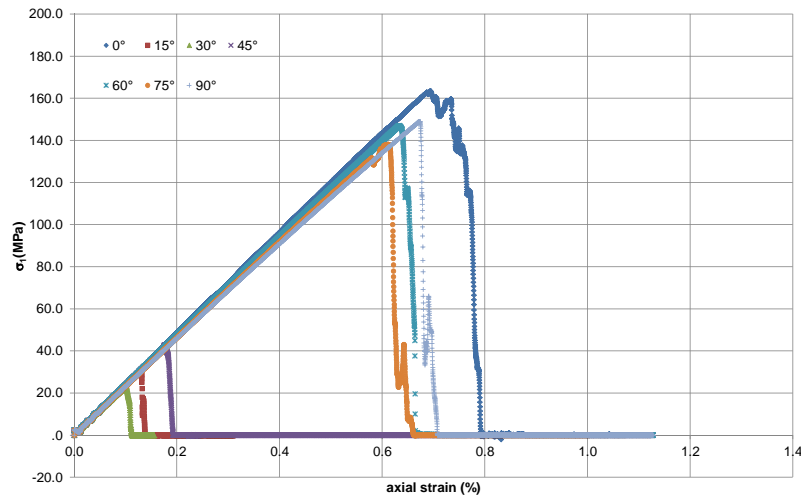
Figure B.17: Stress-strain curves for uniaxial tests of Martinsburg slate specimens with different inclination of joints (β).
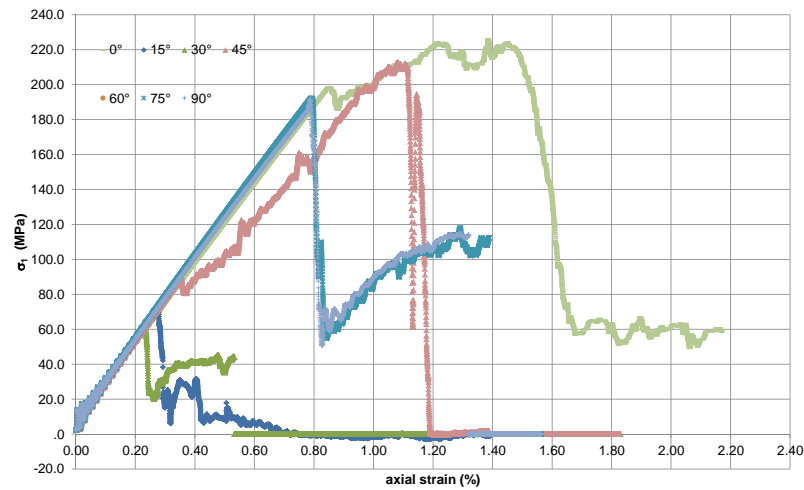
Figure B.18: Stress-strain curves for triaxial tests of Martinsburg slate specimens with different inclination of joints (β).

ing that failure is induced when the normal and shear stress components on the fracture satisfy the Mohr-Coulomb failure criterion, it is possible to develop an expression for the specimen strength as a function of the angle between the maximum principal stress and the normal to the fracture. As shown in Figure B.19 the lowest strength occurs when the discontinuity normal is inclined at an angle of $45°-(\phi_w/2)$ (i.e. $34.92°$) to the maximum applied principal stress.

Figures B.20÷B.22 show some screenshots of uniaxial tests on slate, simulated with the Y2D code. As shown in Figure B.20, the rock specimen exhibit vertical tensile splitting along the joints at the beginning of fracturing, then shear fractures occur. When the angle between the joints and the specimen axis is equal to $30°$, the fractures occur mainly on joints, as shown in Figure B.21. In Figure B.22 the uniaxial test on slate with horizontal joints ($\beta=90°$) is shown; the failure occurs inside the material as shear bands are created, due to the coalescence of single micro-cracks.

Figures B.23÷B.25 show the fracture patterns for the triaxial tests. It is interesting to note that the application of a confining pressure inhibits cracking thus making the samples more ductile. When $\beta=30°$ failure occurs along joints, whereas for $\beta=0°$ and $\beta=90°$ shear bands are created inside the material and lead the specimen to failure.
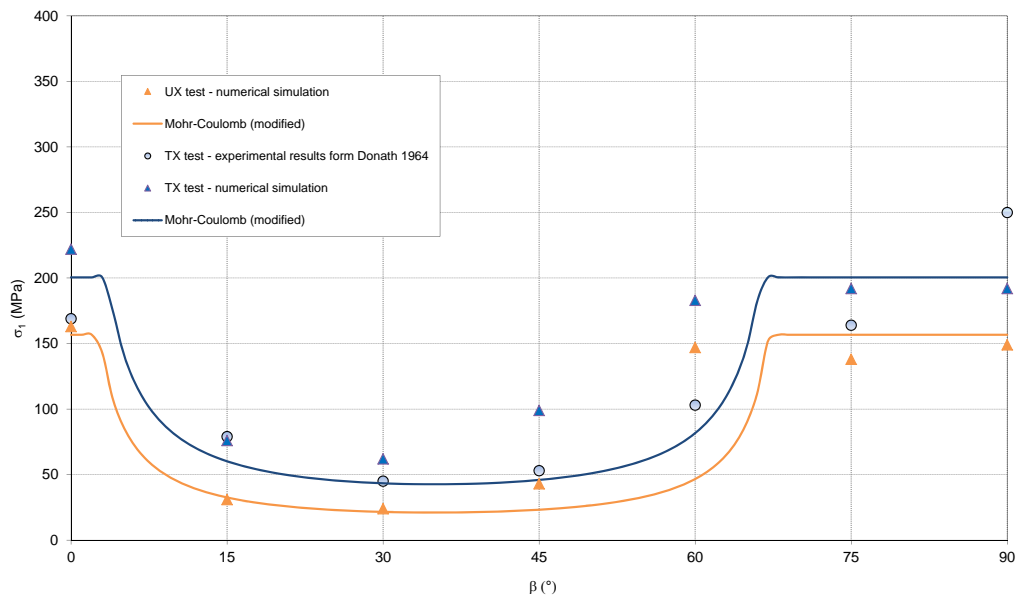
Figure B.19: Influence of anisotropy on rock strength. Comparison among the theoretical curve of Mohr Coulomb modified criterion, laboratory data and the values of the peak principal stress obtained in the numerical simulation of uniaxial and triaxial tests of Martinsburg slate.
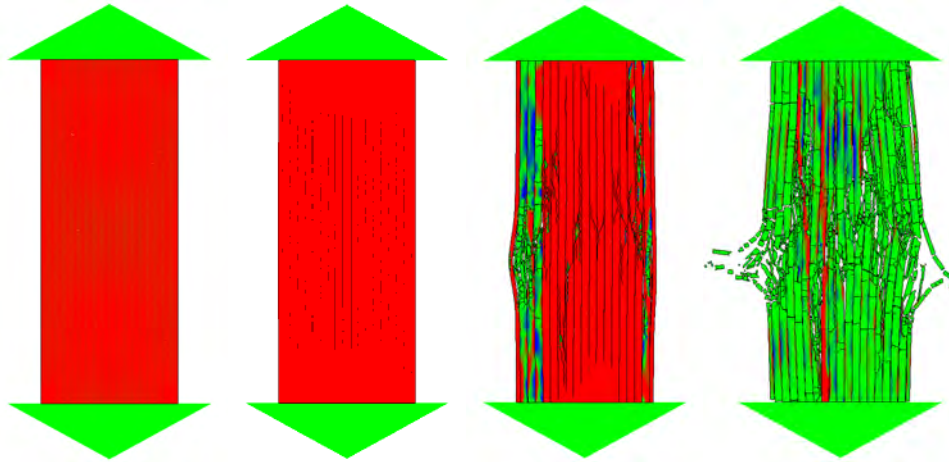
Figure B.20: Uniaxial test of a Martinsburg slate specimen (β=0°): fracture patterns simulated with the Y2D code. Colours represent vertical stresses (red: compressive).
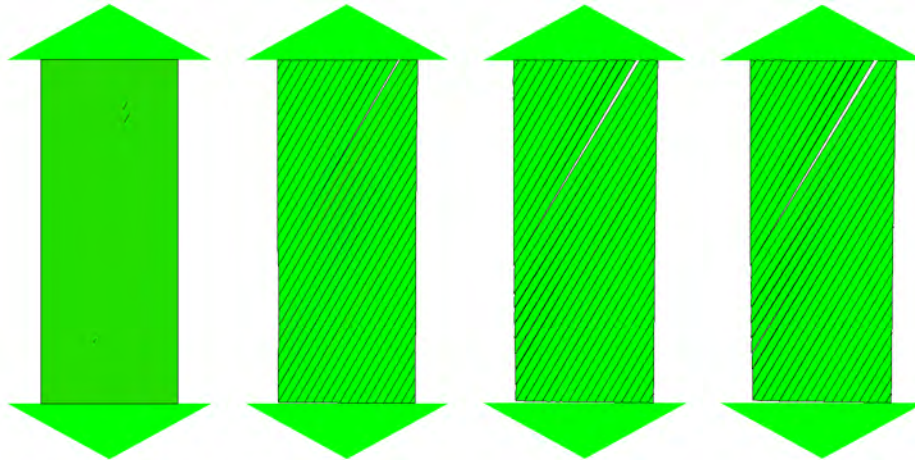
Figure B.21: Uniaxial test of a slate specimen (β=30°): fracture patterns simulated with the Y2D code. Colours represent vertical stresses (red: compressive).
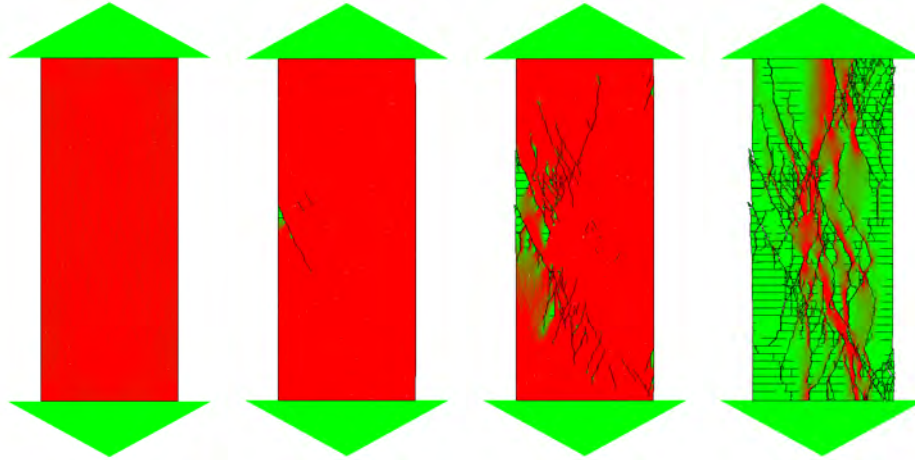
Figure B.22: Uniaxial test of a Martinsburg slate specimen (β=90°): fracture patterns simulated with the Y2D code. Colours represent vertical stresses (red: compressive).
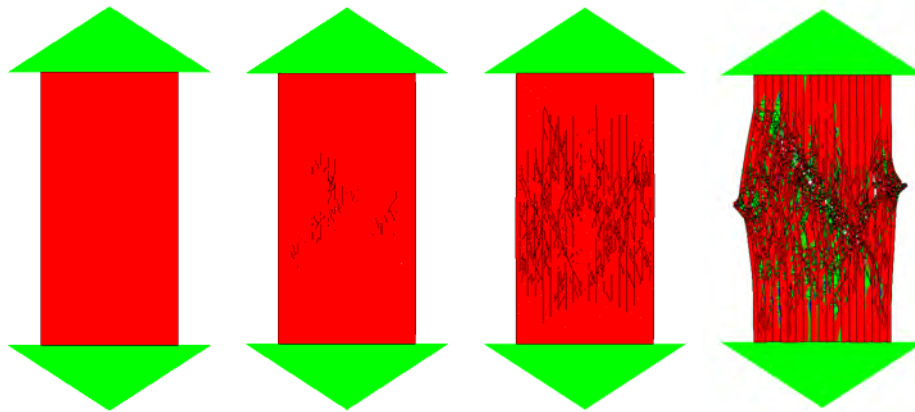
Figure B.23: Triaxial test of a Martinsburg slate specimen (β=0°): fracture patterns simulated with the Y2D code. Colours represent vertical stresses (red: compressive).
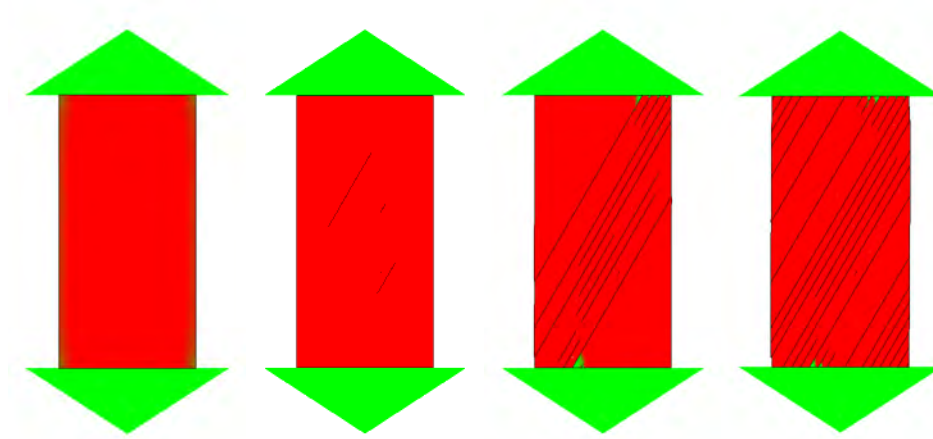
Figure B.24: Triaxial test of a Martinsburg slate specimen (β=30°): fracture patterns simulated with the Y2D code. Colours represent vertical stresses (red: compressive).
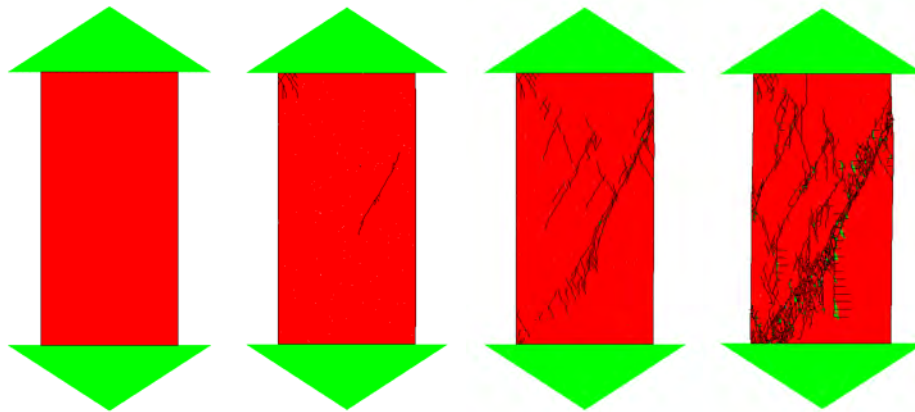
Figure B.25: Triaxial test of a Martinsburg slate specimen (β=90°): fracture patterns simulated with the Y2D code. Colours represent vertical stresses (red: compressive).

B.8   Summary

Anisotropy is a key aspect of rock engineering problems. In a rock mass, the discontinuity frequency can vary very significantly with direction and properties such as the rock mass deformability and strength will be functions of the discontinuity frequency.

For deformability, the architecture of the compliance matrix takes into account the linking between stresses and strains and hence also explicitly quantifies some anisotropy. However, not all rock properties have anisotropy incorporated into their characterization. For example, compressive strength is usually assumed to be a scalar value, which is by definition directionless, but measurement of compressive strength should be qualified with information on the direction of loading relative to the rock structure.

The effect of a single fracture on rock strength can be studied using the single plane of weakness theory which state that the strength of the specimen will then depend on the orientation of the principal stresses relative to fracture orientation.

The numerical simulations presented in this appendix demonstrate the capability of FDEM for quantitatively modelling the failure of a layered rock specimen under uniaxial and triaxial stress conditions. The results obtained from numerical analysis match well with the experimental results and the behaviour of jointed rock mass have been accurately predict.

References

Barla, G., Chiappone, A., and Scavia, C. (**1989**). "Anisotropia di resistenza delle rocce in condizioni di compressione triassiale." *Rivista Italiana di Geotecnica*, 3: 105–120.

Donath, F. (**1964**). "Strength variation and deformational behaviour in anisotropic rocks." In W. R. Judd, editor, "State of Stress in the Earth's Crust," American Elsevier Publishing Co., New York.

Harrison, J. P. and Hudson, J. A. (**2000**). *Engineering Rock Mechanics Part II. Illustrative Worked Examples*. Elsevier Ltd.

Hudson, J. A. and Harrison, J. P. (**1997**). *Engineering Rock Mechanics. An Introduction to the Principles*. Elsevier Ltd.

Jaeger, J. (**1960**). "Shear failure of anisotropic rocks." *Geological Magazine*, 97: 65–72.

Paterson, M. and Wong, T.-f. (**2005**). *Experimental Rock Deformation - The Brittle Field*. Springer.

List of Figures

315

List of Tables